AD-A139 128 ASSESSMENT OF MICRODAMAGE DEVELOPMENT DURING TENSILE LOADING OF GRAPHITE/..(U) VIRGINIA POLYTECHNIC INST AND STATE UNIV BLACKSBURG R D JAMISON ET AL. JAN 84 1/2

UNCLASSIFIED ARO-19913.1-MS-A DAAG29-82-K-0190 F/G 11/4 NL

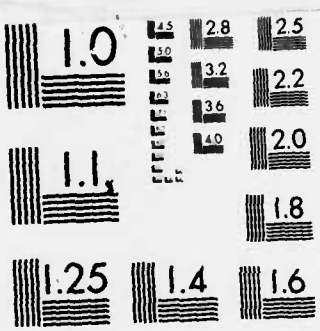

ASSESSMENT OF MICRODAMAGE DEVELOPMENT DURING TENSILE LOADING OF GRAPHITE/EPOXY LAMINATES

FINAL REPORT

RUSSELL D. JAMISON AND KENNETH L. REIFSNIDER

JANUARY 1984

U. S. ARMY RESEARCH OFFICE

CONTRACT NUMBER DAAG29-82-K-0190

VIRGINIA POLYTECHNIC INSTITUTE AND STATE UNIVERSITY

REPORT DOCUMENTATION PAGE	READ INSTRUCTIONS BEFORE COMPLETING FORM
1. REPORT NUMBER	2. GOVT ACCESSION NO. AD-A139 128 / 3. RECIPIENT'S CATALOG NUMBER
4. TITLE (and Subtitle) Assessment of Microdamage Development During Tensile Loading of Graphite/Epoxy Laminates	5. TYPE OF REPORT & PERIOD COVERED Final 1 Sept. 1982 - 30 ~~Aug~~ Nov. 1983
	6. PERFORMING ORG. REPORT NUMBER
7. AUTHOR(s) Russell D. Jamison and Kenneth L. Reifsnider	8. CONTRACT OR GRANT NUMBER(s) DAAG 29-82-K-0190
9. PERFORMING ORGANIZATION NAME AND ADDRESS Materials Response Group, Virginia Polytechnic Institute and State University, Blacksburg, VA 24061-4899	10. PROGRAM ELEMENT, PROJECT, TASK AREA & WORK UNIT NUMBERS
11. CONTROLLING OFFICE NAME AND ADDRESS U. S. Army Research Office Post Office Box 12211 Research Triangle Park, NC 27709	12. REPORT DATE January 1984
	13. NUMBER OF PAGES
14. MONITORING AGENCY NAME & ADDRESS (if different from Controlling Office)	15. SECURITY CLASS. (of this report) Unclassified
	15a. DECLASSIFICATION/DOWNGRADING SCHEDULE

16. DISTRIBUTION STATEMENT (of this Report)

Approved for public release; distribution unlimited.

17. DISTRIBUTION STATEMENT (of the abstract entered in Block 20, if different from Report)

NA

18. SUPPLEMENTARY NOTES

The view, opinions, and/or findings contained in this report are those of the author(s) and should not be construed as an official Department of the Army position, policy, or decision, unless so designated by other documentation.

19. KEY WORDS (Continue on reverse side if necessary and identify by block number)

Composite materials, tensile loading, graphite/epoxy, microdamage, fiber fracture, acoustic emission, radiography, nondestructive testing, strength, stiffness

20. ABSTRACT (Continue on reverse side if necessary and identify by block number)

One of the notable attributes of graphite/epoxy laminates is their high damage tolerance. This quality, however, has served to obscure the precise nature of failure in these materials. While it is recognized that failure results from the nucleation, growth, and coalescence of damage which occurs at the microstructural level, the modes, sequence, and rate of development of this subcritical microdamage are not yet well-understood. The present work examines in a systematic way the development of microdamage in several laminates of

20. Abstract, continued.

graphite/epoxy material during quasi-static tensile loading. Emphasis is placed upon discriminating and quantifying matrix and fiber damage. Penetrant-enhanced X-ray radiography and edge replication were used to map the progression of matrix damage. The recently developed technique of specimen deply was used to follow the progression of fiber fracture. By complementary application of these destructive and nondestructive techniques a more complete and coherent picture of microdamage was developed.

This physical picture of damage development was compared to acoustic emission measurements recorded during loading. Of primary interest was the discrimination between matrix damage and fiber fracture using differences in the amplitude distribution of the acoustic emissions. Correlations are reported for unidirectional and cross-ply laminates.

Table of Contents

List of Tables

List of Illustrations

ASSESSMENT OF MICRODAMAGE DEVELOPMENT DURING TENSILE LOADING OF GRAPHITE/EPOXY LAMINATES

ABSTRACT

One of the notable attributes of graphite/epoxy laminates is their high damage tolerance. This quality, however, has served to obscure the precise nature of failure in these materials. While it is recognized that failure results from the nucleation, growth, and coalescence of damage which occurs at the microstructural level, the modes, sequence, and rate of development of this subcritical microdamage are not yet well-understood. The present work examines in a systematic way the development of microdamage in several laminates of graphite/epoxy material during quasi-static tensile loading. Emphasis is placed upon discriminating and quantifying matrix and fiber damage. Penetrant-enhanced X-ray radiography and edge replication were used to map the progression of matrix damage. The recently developed technique of specimen deply was used to follow the progression of fiber fracture. By complementary application of these destructive and nondestructive techniques a more complete and coherent picture of microdamage was developed.

This physical picture of damage development was compared to acoustic emission measurements recorded during loading. Of primary interest was the discrimination between matrix damage and fiber fracture using differences in the amplitude distribution of the acoustic emissions. Correlations are reported for unidirectional and cross-ply laminates.

KLR:russ-final

Among the significant results is the establishment for the first time of the relationship between applied tensile stress and the *in situ* density and distribution of fiber fractures. Also observed for the first time was the dominant role of matrix cracks in the development of fiber fractures in adjacent load-bearing plies. From the acoustic emission analysis, evidence is provided which questions some common assumptions regarding the relative "strengths" of fiber fracture and resin cracking events in composite materials.

I. Introduction

Carbon fiber reinforced plastic (CFRP) laminates have achieved prominance in a variety of high performance applications. Their high strength and stiffness and low weight make them candidate materials for a broad range of both primary and secondary structures. Among other attributes, this class of material exhibits excellent fatigue resistance. However the development of damage in CFRP, as in other composite materials, is complex and as yet not fully understood. A general understanding of damage development under both static and fatigue loading must be developed if rational predictions of residual strength, stiffness, and lifetime are to be made.

It is becoming increasingly clear that the high damage tolerance which these materials exhibit is attributable to global saturation of certain types of noncritical microstructural damage which develops prior to failure of the laminate [28, 42-45]. It is not, it appears, until very near the end of life that localization of this microdamage begins to occur and a critical prefailure condition develops.

The present work represents a systematic study of the precise nature in which damage initiates, grows, and coalesces during tensile quasi-static loading of certain CFRP laminates. Emphasis is placed upon the study of microdamage, particularly damage relating to resin cracking and fiber fracture. The choice of tensile loading as the damage initiator was made for two reasons. First, the authors and their colleagues in the Materials Response Group at Virginia Tech have developed over the past several years a substantial body of experimental and analytical results for both static and fatigue damage development in composite materials. Although fatigue damage is the more immediate concern of designers and users of laminated structures, an understanding of static damage provides a basis for studying fatigue damage. Although certain damage modes are sometimes suppressed in static loading and the nature and rate of damage growth often differ markedly between the two cases, examination of static damage mechanisms provides valuable insights into the nature of fatigue damage itself.

A second reason for concentrating upon damage due to tensile loading was a practical one. The present work seeks to establish a correlation between individual damage mechanisms and acoustic emission. The bulk of existing experimental and analytical work with acoustic emission to date have been related to static loading. Although some results have been reported for acoustic emission monitoring during fatigue loading [1], the practical difficulties are formidable if one is to attempt to discriminate individual damage modes by this method. One might reasonably expect that only after the practicability of such discrimination has been demonstrated in the relatively benign

experimental environment of static loading would the fatigue case be approachable.

This report is organized as follows: Section II briefly reviews some of the significant previous work in damage characterization and the application of acoustic emission monitoring to damage studies in composite materials. Section III describes the experimental procedure followed and the method of data analysis used. Section IV provides a discussion of results and Section V is a summary of the work and conclusions.

II. Background

A review of much of the previous work in the application of acoustic emission to composite materials is provided in several recent overview papers [2,3]. Some principles of applying AE for damage monitoring are described in references [4-6]. A substantial portion of acoustic emission research in the past fifteen years has been directed to establishing a correlation between one or more attributes of the AE signals and either the quality (absence of defects) or the condition (accumulation of damage) of laminated composite structures. Some of the most extensive research in the former area has involved the proof testing of filament-wound pressure vessels of various materials (7,8]. By the control of certain of the manufacturing variables, this work demonstrated the possibility of distinguishing among populations of "good" and "bad" material as the basis of acoustic emission data recorded during proof testing.

Acoustic emission has also been used successfully as a damage sentinel to indicate the onset of damage. In one recent study [9] the

effect of rubber toughening in a glass reinforced plastic (GRP) laminate was shown, by monitoring AE within a specific amplitude range, to be an elevation of the threshold strain for matrix cracking. Some damage development studies use cumulative count or count rate as the damage sentinel. One recent study of fiber fracture [10] in unidirectional glass and carbon fiber laminates confirmed the usefulness of these parameters to indicate damage incipience and reported correlations between the number of events recorded per fiber fracture and the type of fiber-resin combination used. Fuwa et al. [11] have pointed out, however, that correspondence between the number of AE counts and the number of damage events occurring will not likely exist in any multidirectional laminate where multiple damage modes are operating. A similar conclusion regarding correlation with the mechanical properties was reached in work on cross-ply GRP laminates [12].

Efforts to associate AE with specific damage modes in composite materials have been intensive but not generally conclusive. Several approaches can be identified. One of these is based on the analysis of the frequency spectrum of individual AE events. The assumption is that distinct damage modes produce AE pulses which are themselves distinguishable by their frequency content. Such a view has proven difficult to translate into a workable discrimination technique. Attempts to distinguish fiber fracture from matrix cracking in unidirectional CFRP specimens have met with limited success [13]. The principal difficulty relates to the complex and unknown way in which the AE pulse is changed in passing from the source to the analyzer. The transfer function depends upon both the wave propagation characteristics in the anisotropic, inhomogeneous medium, and the characteristics of the

several electronic stages through which the signal must pass before its frequency spectrum can be analyzed. Although the problem may not be intractable, the practical difficulties are generally recognized to be formidable.

Another approach is the analysis of the AE amplitude distribution. The commercial availability of high rate amplitude sorting instruments has promoted some of the interest in this technique. The technique appeals as well to intuitions regarding the relative "strength" of distinct damage mechanisms. Finally, and perhaps most important in popularizing the use of the method, good correlations between defect and damage growth and AE amplitude distribution have been reported for some specific cases. Harris et al. [14-17] have engaged in extensive and long-standing research programs involving the analysis of AE amplitude distribution from a variety of material systems, loading arrangements and specimen geometries. Their work over the past ten years reflects the development of the technique. Harris and colleagues at Bath University, England have applied the amplitude distribution technique to the quality testing of filament-wound pipes, chopped glass fiber reinforced thermoplastics, and woven and unidirectional laminates in a variety of environments. They have reported correlations between specimen condition (defect density or environmental degradation) and certain attributes of the AE amplitude distribution recorded during loading of these specimens. Their work in discriminating among damage mechanisms in specimens of the same quality has not to date produced such correlation. These efforts have nonetheless established a firm basis for future work. In critically examining certain widely-held

presumptions about AE-damage relationships, they have shown some to be misleading, others false.

For example, it has been suggested that if the energies of emissions, a, are randomly distributed, the cumulative distribution, n(a), will be of the form,

$$n(a) = (a/a_o)^{-b}$$

where a_o and b are constants. In a homogeneous material, a large value of b would indicate emissions from a large number of small amplitude events whereas a small value of b would indicate predominantly high energy events. Presumably then a change in the source of AE events would be revealed by a change in b. Although claims to this effect have been made [18,19], Guild et al [12] have demonstrated that such discrimination on the basis of the b parameter is not generally possible. The released energy of fiber fracture for example is ultimately related to the condition of the interface at the fracture site. The energy released in resin cracking is related intimately to the properties of the resin as well as to the constraint of adjacent plies. Their work has snown in fact that a single value of b will adequately describe a range of different damage mechanisms.

Awerbach [20] and Block [21] have reported preliminary results of ambitious programs to study damage progression in CFRP laminates using a complement of acoustic emission characteristics: cumulative events and event rates; event amplitude, energy, and frequency spectra; and source location. Such programs are necessarily broad and long-term. When coupled with thorough damage characterization, these studies may place

one or more of these techniques on firmer ground and contribute to a better understanding of damage development in composite materials.

It is only in the union of thorough, systematic damage characterization and rigorous, critical acoustic emission analysis that the full potential of this valuable evaluation technique can be realized. There presently exists a large body of results from analytical and experimental efforts to characterize various composite damage mechanisms: ply cracking [22-26], fiber fracture [27-28] and delamination [29-30] for example. However without the benefit of a collateral effort to characterize the acoustic emission associated with the development of this damage, the development of AE monitoring as a reliable damage identification technique is not likely to be possible. Conversely, with some notable exceptions, elegant analysis of acoustic emission data is sometimes accompanied by cursory or hypothetical treatment of the damage state. The tacit acceptance of prejudices about damage mechanisms will impede the ultimate appraisal of the acoustic emission technique as a reliable damage monitor and discriminator. It is only when both aspects are treated with equal rigor that present questions about the value of acoustic emission analyses in damage studies can be properly addressed.

III. Experimental Procedure

Specimens were prepared from prepreg material supplied by Fothergill and Harvey. Fibers were T300 and resin was Code 91, a proprietary Fothergill and Harvey resin similar in composition to Ciba-Geigy 914C and NARMCO 5208 but having a lower curing temperature. Plates measuring 457mm x 457mm were manufactured at the autoclave

facility of the Royal Aircraft Establishment, Farnborough, England. Each plate was ultrasonically C-scanned after fabrication to ensure consistent quality. Specimens measuring 203mm long by 25mm wide were cut from the plates using a diamond impregnated, wetted circular saw.

All tensile testing was performed on an Instron 1195 screw-driven machine having a capacity of 50 kN in a displacement-controlled mode. Crosshead displacement speed was 0.5mm/min which corresponded to a strain rate of 1.7×10^{-4}/sec. Strain was measured by an extensometer having a nominal gage length of 12.5mm, attached with elastic bands to one face of the specimens. Gripping was accomplished using Instron mechanical wedge grips. Ends of specimens were built up with a 0.1 mm thick layer of epoxy as reinforcement and protection from wedge face damage.

Two stacking sequences were used: $[0_2]_s$ and $[0,90_2]_s$. Two series of the cross-ply laminates were produced. The first series was of low porosity. The second series, through a modification in the cure schedule by which application of pressure was delayed, exhibited significant porosity. The volume fraction was nominally 62% for all specimens.

There were therefore three populations available for characterization and analysis: two having nominally the same defect state but different stacking sequence ($[0_2]_s$ and $[0,90_2]_s$, both non-porous) and two having the same stacking sequence but significantly different initial defect states ($[0,90_2]_s$ porous and $[0,90_2]_s$ non-porous).

Characterization of the effect of tensile loading on damage development in these populations was accomplished in two ways. First was

an examination of specimens loaded to increasingly greater fractions of the mean ultimate stress ($\bar{S}_{ult}$) in order to identify the modes of damage which developed and to determine their incipiency levels, growth rates and interactions. This characterization was accomplished using the nondestructive techniques of edge replication and X-ray radiography and the destructive techniques of sectioning and specimen deply.

The second characterization was of the acoustic emission. A series of specimens was loaded to tensile failure and the AE was recorded and stored on a computer-interfaced system for subsequent analysis of the amplitude distribution of events. The acoustic emission results were then compared to the damage chronology to seek correlation between attributes of the amplitude distribution and individual damage modes.

Brief descriptions of the damage characterization techniques and the acoustic emission analysis are provided in the following sections.

Edge Replication

Edge replication of composite specimens has been employed with considerable success in the study of ply cracking and edge delamination [31]. In order to use the technique effectively for composite materials, the specimen edge must be polished with successively finer grades of silicon carbide paper and powdered alumina. To produce a replica of a polished edge, a piece of cellulose acetate tape, 10 mils in thickness, is affixed to the specimen edge with adhesive tape. A small amount of acetone is injected between the tape and specimen and the tape is pressed quickly and lightly against the specimen edge. The acetate tape is allowed to harden for approximately one minute and upon removal retains a permanent, high fidelity replica of the edge

topography. The replica is mounted and labelled on a glass place for inspection and storage. Examination of the replica can be accomplished in several ways. One means is by use of a microfiche reader which provides magnification on the order of 20-50x. This is more than sufficient to distinguish the details of ply cracking and delamination which occur at the edge.

X-ray Radiography

Penetrant-enhanced X-ray radiograph is a common NDE technique for the characterization of damage in composite materials. The penetrant chosen for the present work was zinc iodide in a carrier of dilute isopropyl alcohol. This penetrant exhibits excellent X-ray opacity and diffusivity in graphite/epoxy material and is notable for its atoxicity in humans. Although this agent is naturally diffusive into damage zones, penetration was greatly improved by applying the zinc iodide solution along the specimen edge while the specimen was oriented horizontally and subjected to a small tensile load. This was accomplished by using an arrangement similar to the one shown in Fig. 1. The specimen was clamped in the loading fixture with one specimen edge uppermost and loaded to approximately 1 kN. Two strips of adhesive tape extending approximately 6mm above the edge were fastened to the specimen surfaces. Plates were clamped over the top flush with the specimen edge to ensure a seal with the surface and the ends of the tape were crimped shut. A small amount of stopcock grease was injected at each end to provide a viscous plug. The channel thus formed was filled with the zinc iodide solution which was allowed to remain at least thirty minutes. Both edges were treated in the same manner.

An X-ray instrument was not available at Bath University. However a Phillips Type BV-21-S X-ray unit was made available by the Area Medical Physics Group at the Royal United Hospital in Bath. X-ray radiographs were made at 25KV and 3ma. Exposure times depended upon the laminate thickness and varied between 60 and 90 seconds. Film-to-source distance was approximately 300 mm. The film used was Kodak Industrex MX, a high resolution, double emulsion film.

Sectioning

Sections were taken perpendicular to the long axis of specimens to examine fiber/matrix disbonding in the 0 degree plies. Sections were taken parallel to the specimen long axis in $[0,90_2]_s$ laminates to examine microcracking in the 90 degree plies. All sections were mounted in resin and polished metallographically using successively finer grades of wetted silicon carbide paper and alumina powder. Sections were examined in both optical and scanning electron microscopes.

Specimen Deply

Efforts to study fiber fracture in the interior of laminated specimens pose difficulties for available NDE methods. Since this information is essential for the complete characterization of damage, a destructive, microscope technique developed by Freeman [29] was employed in the present work. In this method, the specimen is heated to a temperature sufficient to partially pyrolyze the resin matrix. The interlaminar bond strength is thereby diminished to the extent that the individual plies of the laminate can be separated. For T300/Code 91 graphite/epoxy material, the required temperature is 450°C. The time

required depends upon the laminate thickness: for 6-ply laminates, 50 minutes was used; for 8-ply laminates, 70 minutes. The heating was accomplished in an electric oven. The process evolved noxious fumes in quantity which were evacuated from the oven and vented outside. The specimen was removed from the oven after the required time and allowed to cool in air.

By the use of a small knife edge and pointed probe, the individual plies could then be separated. Sufficient resin material remains after pyrolysis to hold the plies together if they are handled carefully. For the present study, coupons were cut from the deplied laminae for SEM examination so that the details of fiber fracture could be studied. Working magnifications for the study of patterns of fiber breaks was 200-400x; to study the details of individual fiber fractures, 1600-200x magnification was required.

Acoustic Emission Monitoring

Acoustic emission was monitored during the loading of most specimens. The evaluation of this "damage analog" information proceeded in parallel with the physical damage characterization. The acoustic emission monitoring system consisted of a wide band PZT transducer having a circular contact diameter 25.4mm coupled to the specimen with Dow Corning silicone grease and clamped mechanically to the center portion of one of the specimen faces. The transducer output passed through a 60 dB preamplifier which contained a 100 kHz to 1 MHZ band pass filter into an AETC Model 203 Amplitude Analyzer manufactured by Acoustic Emission Technology Corporation. This system covers an amplitude range from 20 μV to 20 mV at the sensor (26 dB to 86 dB with

respect to 1 μV at the sensor). The analyzer divides this range equally into 50 channels, each of width 1.2 dB. The threshold of the instrument can be raised above 20 μV and channels eliminated by a switch setting to filter some low amplitude background noise. In the present work channels 0-3 were excluded in this way giving an effective threshold of approximately 30 μV at the sensor. The AETC system operates also as an event counter capable of distinguishing one event from the next provided there is a dead time of at least 100 μS between successive events. For a typical pulse of 400 μS, the system is intrinsically capable of registering 2000 events per second. A primary reason for testing at very low strain rates was to stay within this limitation and avoid the loss of information near failure when large count rates were generally observed.

Previous experience with this equipment at the University of Bath had shown that an expanded data collection, management, and storage capability was necessary if the full benefit was to be derived from the acoustic emission measurements. The AETC 203 equipment had therefore been interfaced with a Digital Equipment Corporation MINC-11 computer so that all significant test parameters were recorded on a time-resolved basis. Upon completion of a test the analog load and strain signals and digital acoustic emission amplitude data which had been recorded on a floppy disk were transferred to a Prime 750 computer at the Rutherford Appleton Laboratory (RAL) for later processing and analysis. The principal processing medium was a set of highly flexible plotting routines in which any of the test data could be provided in any combination in graphical display at a VDU or in hard copy via a peripheral plotter facility at RAL. Inasmuch as the data was archived

at RAL and retained in the disk medium, individual tests remained accessible for subsequent analysis by improved or modified analysis techniques or for cross-correlation with data from other tests. A complete description of the data collection and processing system is contained in reference [17].

IV. Results and Discussion

Results of preliminary mechanical testing of specimens from the porous and non-porous $[0,90_2]_s$ and non-porous $[0_2]_s$ populations are summarized in Table 1. Six specimens were tested in each group. The average ultimate strength of the porous cross-ply laminates was 11 percent lower than the non-porous cross-ply laminates but showed no greater variability in measurement. The average void content of the porous specimens was consistent with the excessive porosity observed at the edge of these specimens. The void content of the non-porous specimens was too small to be measured accurately.

Results are presented in this section in two groups. First the non-porous cross-ply and unidirectional specimens are compared in terms of damage development and AE characteristics. Second, the non-porous cross-ply and porous cross-ply laminates are compared in a similar way.

$[0,90_2]_s$ and $[0_2]_s$ Non-porous Laminates

$[0,90_2]_s$ Damage Development

When cross-ply laminates of most fiber-reinforced composite materials are subjected to tensile loading they experience transverse ply cracking. In CFRP laminates such cracks can begin at relatively low stress levels and typically have a brittle character, growing very

rapidly from edge to edge and through the 90 degree ply thickness. Figure 2 is a series of penetrant-enhanced X-ray radiographs of non-porous $[0,90_2]_s$ laminates loaded to successively higher stress levels. At loads below 30 percent of the mean ultimate load, cracks were not observed. At loads above this level, cracking occurred and the density of cracks increased with increasing load. Figure 3, an enlargement of Fig. 2b, shows the regularity of these cracks, characteristic of CFRP.

The development of cracks in off-axis plies of laminates subject to tensile loading has been studied extensively [22-26]. The development of a saturation spacing of such cracks has been predicted analytically and observed experimentally [32]. This condition which imposes an upper bound on crack density has been termed the characteristic damage state [22]. It has been shown to be dependent upon the properties of each ply, their thickness, and the stacking sequence of plies but independent of the load history, [31, 32, 43-45].

Figure 4 shows the relationship between tensile load and the density of transverse ply cracks in $[0,90_2]_s$ specimens. For these measurements several specimens were loaded incrementally to successively higher loads. After each load increment, the load was reduced and edge replicas were made. Cracks were counted over a 25.4 mm gage length from the replicas under a microscope. A marked increase is observed from Fig. 4 in crack density at a load of approximately 45 percent of the average ultimate load, $\bar{S}_{ult}$. Beyond this level, the crack density increases more gradually toward a predicted saturation level of 13.8 cracks per cm. This predicted density is based on a one-dimensional

shear lag analysis developed by Reifsnider et al. and described in detail in [43].*

In this method of crack density measurement, sufficient time is allowed for cracks to fully develop at each load level. The time dependence of crack development follows from the viscoelastic behavior of most polymer resins at ambient temperatures. To study this effect in greater detail for the T300/Code 91 system used in this investigation, one $[0,90_2]_s$ specimen was loaded to 70% $\bar{S}_{ult}$ and maintained at that level. Replicas were made at selected time intervals between one minute and sixteen hours. The results are shown in Fig. 5. After 10 minutes under load the crack density reached 9.9 cracks per cm. After 42 minutes the density had not increased and after 1000 minutes at the constant load, the crack density was 10 cracks/cm.

In quasi-static loading, the rate of loading is often limited by the range of the testing machine used. In screw-driven, displacement-controlled machines operating in the lowest range, the rate of loading can be such that full crack development does not occur at any given load. That is, the time required for crack formation to be complete at a given load may not be available. Since one aspect of the current work was the correlation of crack development with the acoustic emission produced during loading, it was necessary to establish the "quasi-static" crack density vs. load relationship for the loading rate actually used.

---

* An average crack density of 12.6 cracks/cm was measured for several specimens taken from this population and subjected to 100-200 thousand cycles of tension-tension cyclic loading, reconfirming the load history independence of the saturation density.

A number of non-porous specimens were loaded individually to various levels between 30 percent and 104 percent of the average ultimate stress and unloaded immediately. The rate of crosshead displacement for loading and unloading was 0.5mm/min, the same rate used in all subsequent tensile loading and the lowest rate available on the testing machine. For $[0,90_2]_s$ specimens this corresponded to a loading rate of approximately 0.02 kN/sec. Each specimen was loaded only once and unloaded without a dwell time at load. Edge replicas were made at a load of 30% $\overline{S}_{ult}$ (below the cracking threshold) and crack densities were measured as described previously.

Figure 6 shows this load vs. crack density relationship. Both the crack density magnitudes and the shape of this curve are different from the previous results. At every load level the crack density was lower than the apparent equilibrium value -- 38 percent lower on average at 100% $\overline{S}_{ult}$. The curve shows no rapid increase at 40-50% $\overline{S}_{ult}$ as previously observed and in fact has an overall shape suggesting a power law relationship.

The relatively low crack densities measured in specimens near failure was reflected in specimens which were replicated after failure. In fact the five post-failure specimens replicated displayed an average crack density approximately the same as those replicated near failure and significantly lower than the 12.1 cracks/cm indicated in Fig. 2.

For the purposes of acoustic emission analysis, the crack density-load relationship shown in Fig. 6 was taken to be representative of the actual rate of crack development during quasi-static loading. As will

be shown, such a relationship is consistent with the cumulative acoustic emission measured.

With the crack density-load relationship established, the characteristics of the cracks themselves were examined. Figure 7 shows at successively higher magnification typical cracks which developed at a tensile load of 102% $\bar{S}_{ult.}$ As observed previously, the cracks are continuous across the width (see Fig. 3) and have grown in an essentially self-similar manner. They have generally passed around fibers in their path and extend into the resin-rich region at the 0/90° interfaces. Significantly they have not turned along the interface to produce a delamination as is often observed in tension-tension fatigue loading of CFRP laminates. In regions of the transverse plies away from crack, there was no indication of resin microcracking or fiber-matrix disbonding. For specimens loaded to 30% $\bar{S}_{ult}$, just below the level for crack incipience, there was likewise no evidence of microcracking or disbonding anywhere in the transverse plies. An edge section of such a specimen is shown in Fig. 8.

The scanning electron micrograph of a transverse crack surface shown in Fig. 9 displays the glasslike appearance characteristic of brittle fracture in the resin. Here, too, it is seen that the crack remains in the resin phase, leaving the fibers sheathed in resin. This latter effect is related to the fiber surface treatment, if any, and may vary accordingly. It has however been observed in both T300/5208 and T300/Code 91 systems by the present investigators.

Transverse ply cracking in these non-porous cross-ply laminates can thus be characterized as a brittle process which proceeds nearly instantaneously producing an essentially planar surface entirely within

the resin phase. Moreover, sections of cracked laminates, taken both at the free edges and at the interior do not show the presence of fiber/matrix disbonds in the transverse plies at any load level. Such microcrack precursors of fully developed transverse ply cracks have however been reported [24] for certain cross-ply laminates fabricated from an unidentified graphite/epoxy system. It is likely that the fiber/matrix bond plays a dominant role in determining the precise nature of the nucleation and growth of transverse ply cracks.

The large Poisson mismatch between the 0 degree and 90 degree plies in a cross-ply laminate cause relatively large transverse stresses to be produced in the 0 degree plies when the laminate is subjected to a tensile load. These stresses can approach or exceed the ply strength in the transverse direction [24,28]. Radiographs of specimens loaded between 30 percent and 100 percent of the ultimate strength were examined for evidence of longitudinal cracking. Even for specimens loaded to 100% $\bar{S}_{ult}$, no longitudinal cracks were observed in the radiographs. Sections of specimens taken perpendicular to 0 degree fiber direction were prepared. Longitudinal cracks were not observed at any section for any load condition.

Such a results is consistent with the σ_y stresses in the 0 degree plies calculated from the classical laminated ply theory. The predicted σ_y stress at laminate failure, 25.5 MPa, is substantially less than the transverse strength of the 0 degree plies, 44.8 MPa. It should be noted that longitudinal cracks have been observed to occur during cyclic loading of T300/5208 $[0,90_2]_s$ laminates at stresses will below the failure level [33]. This damage mode is in fact of considerable

significance in the overall fatigue damage development of these laminates.

The state of fiber fracture in the 0 degree plies was examined as well so that the relationship between load and fiber fracture density could be determined. Using the technique of specimen deply, the 0 degree plies of laminates loaded to various fractions of the ultimate tensile strength were "unstacked" from the laminate. Portions of these plies were examined in a scanning electron microscope and the average fiber fracture density was calculated by counting broken fibers in a large number of randomly selected representative areas. The process of deplying, if done with care, produces very few fiber fractures. Virgin specimens were deplied and the average fiber fracture density was calculated. This measurement provided a basis from which the true relationship between load and fiber fracture density could be determined.

The deply technique is a destructive one and several specimens were required at each load level to develop the load-fiber fracture relationship. The counting process was tedious but unambiguous. Figure 10 is a typical single frame of a representative area. The overall dimensions of each representative area was fixed at 10 frames by 10 frames (7 mm x 5 mm). At the operating magnification of 270x, individual fiber fractures were distinct. At higher magnifications, details of the fiber fractures could be studied.

Previous work by the authors [33] had established for the first time that in tension-tension fatigue loading of composite laminates, fiber fractures were not randomly distributed as the fiber strength distribution would predict. They were instead confined to narrow zones

outside of which few fiber fractures were observed. The location of these zones was found to coincide precisely with the location of cracks in adjacent plies. Figure 11 is a schematic representation of this pattern.

Such a pattern of ply cracking-induced fiber fracture was observed in all of the cross-ply laminates subjected to tensile loading in the present work as well. That is, in tensile loading of CFRP laminates, off-axis ply cracks are the dominant influence upon the location of fiber fractures in adjacent plies regardless of the tensile load history.

Details of these fiber fractures are shown in Fig. 12. Fractures had a clear cleavage-like appearance in most cases and often occurred in clusters. This multiplicity of fiber fractures has been anticipated by numerous unidirectional strength models [34-36] and has been observed in certain translucent resin/glass fiber systems. It was also observed by the present authors in fatigue-damaged CFRP laminates. This aspect of the present work is of particular interest in light of recent models which predict laminate failure on the basis of the development of a critical "multiplet" of adjacent fiber fractures anywhere in one of the critical load-bearing plies. Consequently both the density and the multiplicity of fiber fractures was determined over the range of load levels to failure.

Figure 13 shows the fiber fracture density-load relationship for the non-porous $[0,90_2]_s$ laminates. This is the first time, to the authors' knowledge, that such a relationship has been determined experimentally for any CFRP material by direct observation of fiber fractures <u>in situ</u>. Previous attempts at quantifying fiber fractures by

acid leaching of resin in Boron/Epoxy laminates [37], or by observing local crazing at broken glass fibers in translucent epoxy matrices [27], have lacked the advantage of direct access to the sites of fiber fracture provided by the deply technique. The data from which Fig. 13 was developed are provided in Table 2.

Figure 13 shows that for tensile loads below 70% $\overline{S}_{ult}$ there are essentially no broken fibers in excess of those found in virgin specimens. At loads above this level, the fiber fracture density increases rapidly, reaching 107 fiber fractures/representative area at 100% $\overline{S}_{ult}$ and 129 at 102% $\overline{S}_{ult}$.

In summary of the damage characterization for the non-porous $[0,90_2]_s$ laminates, there are two principal damage mechanisms operating: transverse ply cracks which initiate at tensile loads above 30% of the ultimate strength and which increase in density metastably in an approximate power law fashion; and fiber fractures which initiate at approximately 70% $\overline{S}_{ult}$ and also increase in density in an approximately power law form with increasing load.

Secondary microstructural damage modes such as fiber-matrix debonding, resin microcracking, or longitudinal cracking were not observed at even the highest load levels.

$[0,90_2]_s$ Acoustic Emission Analysis

Figure 14 shows for reference a composite of the fiber fracture and transverse cracking versus load relationships. The vertical scales have been normalized to facilitate comparisons. Figure 15 shows the cumulative acoustic emissions recorded during the loading of a typical non-porous $[0,90_2]_s$ specimen over the same range. Both the total event

and event rate curves exhibit a functional relationship suggestive of the damage relationships of Fib. 14. The lack of evident fine structures in these curves however diminishes their usefulness in discriminating between the principal damage modes which have been seen to act in this laminate type.

Figure 16 shows two presentations of the amplitude distribution of the acoustic emission in each of six load ranges for a typical specimen. The load ranges used as a basis for comparison of the AE amplitudes were defined as follows:

Load Level	Load Range (% $\overline{S}_{ult}$)
1	0 - 30
2	30 - 60
3	60 - 70
4	70 - 80
5	80 - 90
6	90 - Pre-failure

These load level references will be used throughout the succeeding discussion of results. In load ranges 1 and 2 which together extend from no load to 60% $\overline{S}_{ult}$, the amplitude distribution is inclusive of channels 4-20. These are the load ranges in which cracks are occurring prior to a significant amount of fiber fracture. In load range 3 (60-70% $\overline{S}_{ult}$), ply cracking activity has increased and remains the predominant active damage mode. The amplitude distribution for this load range includes a small but significant number of events in channels 20-30. In load range 4 (70-80% $\overline{S}_{ult}$) where cracking continues and fiber fracture begins, the amplitude distribution exhibits a small shift toward the channels in the range between 15 and 30. With increasing load in ranges 5 and 6 (80% $\overline{S}_{ult}$ - failure), the amplitude distribution

remains essentially unchanged. This is the load range over which both damage mechanisms are operating simultaneously. (It should be noted that range 6 includes events which occurred prior to fracture but does not include events which occurred during the actual fracture process. This acoustic emission of "rending" has thus been excluded in the present analysis.)

These patterns which were observed when the acoustic emission was examined by load range, although subtle, were highly repeatable. Figure 17 for example shows the amplitude distributions for the acoustic emission recorded during the tensile loading to failure of another $[0,90_2]_s$ specimen taken from the same non-porous population but tested at a different time. The similarity with Fig. 16 is notable.

In choosing amplitude distribution as the characteristic of the acoustic emission to be used in discriminating one damage mechanism from another, the implicit assumption was that fundamentally different damage mechanisms (e.g. transverse ply cracking and fiber fracture) would not likely produce acoustic emissions having identical amplitude distributions. When these mechanisms are operating simultaneously over a significant portion of the load spectrum, the problem becomes one of determining the distribution due to each mechanism separately and thence deconvoluting the superposed distributions actually observed.

Clearly from the results of the known sequence of ply cracking and fiber fracture in non-porous $[0,90_2]_s$ laminates and the amplitude distributions shown in Figs. 16 and 17 this is not a simple matter. The intuitive concept that fiber fracture is by its nature a higher energy event than ply cracking and therefore produces higher amplitude acoustic emission is difficult to reconcile with the present results. In the

range of loading over which transverse ply cracking is the dominant active damage mechanism (30 - 70% $\bar{S}_{ult}$), the amplitude distribution is clearly not shifted to lower amplitudes with respect to the distribution of amplitudes over the load range 70% $\bar{S}_{ult}$ - failure when fiber fractures begin to occur. Indeed, it is at these higher loads, near failure, where a slight shifting to lower amplitudes is observed.

This phenomenon is perhaps better seen in a slightly different presentation of the same data used to produce the amplitude histograms of Fig. 16. Figure 18a shows the relative distribution of events which occurred in selected channel ranges as a function of load. The channel ranges were chosen arbitrarily to be:

Range Number	Channels Included
1	4 - 9
2	10 - 15
3	16 - 21
4	22 - 27
5	28 - 33
6	34 - 50

At low loads there are few total counts and the interpretation is not meaningful. But as the first significant damage begins to occur, (at loads between 4 and 6 kN) the share of events in the lowest channel range begins to diminish. In this range (channels 4-9) are included spurious, low amplitude background events which occur independently of the load as well as a sizable number of the actual damage-generated acoustic events. As channel range 1 decreases its share of the total, channel ranges 2-5 increase their relative share of the total cumulative events. This trend becomes significant at loads around 8 kN (approximately 65% $\bar{S}_{ult}$) when ply cracking becomes increasingly

active. This is seen more clearly in Fig. 18b which shows the same analysis plotting, only events occurring in channels 10 through 50. Significantly, the proportion of events in the highest channel range is seen to begin to diminish at loads above 10 kN and to continue to diminish through failure. This is the load range over which nearly all fiber fractures are occurring.

Such behavior is inconsistent with the assumption that fiber fracture is the source of higher amplitude acoustic emissions. Indeed as the rate of fiber fracture is greater than the rate of ply cracking in the higher load ranges, it could be concluded that transverse ply cracking is the principal contributor of the higher amplitude events and in becoming proportionately a smaller fraction of the total cumulative damage as load is increased, its higher amplitude contributions to the cumulative acoustic emission would likewise become proportionately smaller.

These patterns were identified repeatedly in similar plots for other specimens tested. Figure 19, representative of another specimen loaded to failure, demonstrates the reproducibility of these relatively small changes in the amplitude distributions. In all cases, without exception, the proportion of events occurring in the highest amplitude range recorded during tensile loading to failure of $[0,90_2]_s$ laminates diminished as the specimen neared failure.

In summary of the results of this section, discrimination between ply cracking and fiber fracture based on analysis of the amplitude distribution of the acoustic emission produced requires that quite subtle distinctions be made. These distinctions in the evolution of the amplitude distribution with increasing load are nonetheless clear and

repeatable. The range of amplitudes which one might assign to transverse ply cracking would not be substantially different from that assigned to fiber fracture based upon results for this laminate and this material. It is clear that the onset of the first dominant damage mode can be detected with good accuracy. The amplitude distribution proved to be a more sensitive sentinel of transverse ply cracking incipience that either the cumulative count or count rate.

However identification of damage modes based solely upon attributes of the amplitude distribution of the associated acoustic emission is more difficult. And when several modes are occurring simultaneously (albeit at different rates) the discrimination problem is formidable.

In the present instance, discrimination between ply cracking and fiber fracture, perhaps the most physically distinguishable pair imaginable, requires a conclusion that ply cracking is a slightly higher amplitude event on average than fiber fracture. Such a conclusion must be qualified inasmuch as both damage mechanisms are acting simultaneously. Results presented in the next section seek to clarity the individual characteristics of the damage modes by isolating fiber fracture.

$[0,0]_s$ Damage Development

The testing procedure for the $[0,0]_s$ laminates was identical to that used for the cross-ply laminates. Specimens were loaded to various fractions of their average static tensile strength, unloaded and examined. Radiography is not particularly useful for revealing damage in unidirectional laminates because of the difficulty in achieving

penetrant-enhancement. Therefore the principal methods of damage assessment were sectioning and the deply scheme.

Sections taken normal to the fiber direction in specimens representative of the complete load range through failure were examined for evidence of longitudinal cracking. It was recognized that uniaxial specimens in general and CFRP laminates in particular are prone to this type of damage owing to shear stresses produced in gripping and the low shear strength of epoxy resins. However an extensive section study for the specimens used in the present research produced no evidence of longitudinal cracks. Sections examined in both light and electron microscopes showed no evidence of either cracks or fiber/matrix disbonds even for specimens loaded to 103% $\bar{S}_{ult}$. Only in one section, taken from a specimen loaded to 102% $\bar{S}_{ult}$, was disbonding observed. It was confined to small clusters of fibers. There was also some evidence of microcracking in the resin between these fibers. However this was an isolated observation. The overall indication was that cracks did not develop prior to fracture in these unidirectional specimens and that if fiber/matrix disbonding occurred, it did so only at load levels approaching the failure mode.

Consequently the dominant damage mode was fiber fracture. The relationship between tensile load and the density of these fiber fractures was determined in the same manner described for the cross-ply laminates. The result is shown in Fig. 20 along with the result for the $[0,90_2]_s$ laminates for comparison. Just as for the $[0,90_2]_s$ case, a significant number of fibers do not fracture until a load of approximately 70% $\bar{S}_{ult}$ is exceeded. The fiber fracture density then increases rapidly with increasing load through failure.

Inspection of Fig. 20 would suggest that the density of fiber fractures at failure is substantially higher in the cross-ply laminate. While this may in fact be true, the difference would be less than that shown. The method of counting fiber fractures used to produce these curves has undoubtedly exaggerated whatever real difference there may be. In the cross-ply laminates, fiber fractures were counted in the fiber layer adjacent to the 0/90 interface and hence nearest to the crack tip. It has been shown by the authors in previous work [34] that the density of fiber fractures is markedly diminished in fiber layers away from the interface, 70% fewer only one fiber diameter removed from the interface in the case of fatigue. Although it is possible to remove fiber layers from the deplied laminae by the application and careful removal of pressure sensitive tape, the number of observations required to produce meaningful fracture density statistics precluded through-thickness accounting. It is possible therefore to conclude only that fiber fracture density observed at the interface is higher in cross-ply laminates than in unidirectional laminates at comparable stress levels.

Figure 21 is another presentation of the same data in which the fiber fracture densities are plotted against the measured strain magnitude. Assuming linear elastic behavior of the 0 degree plies to failure, the measured strain is proportional to the stress in the 0 degree plies. Hence Fig. 21 provides a comparison between fiber fracture density in the 0 degree plies and the stress in those plies. Here the influence of the transverse ply cracks upon fiber fracture in cross-ply laminates is clearly observable. Fiber fractures initiate at slightly lower stresses and increase at a faster rate over a range of elevated stress. However, the rate of fiber fracture very near failure

in unidirectional plies exhibits a rapid increase and approaches or exceeds the cross-ply rate.

The fiber fracture density in the unidirectional laminate can be used to estimate the cumulative number of fiber fractures which occur up to laminate fracture. Using the representative area dimensions of 7 mm x 5 mm, ply dimensions 25 mm x 100 mm, and thickness of 88 fibers (4 plies x average 22 fibers per ply) and a fiber fracture density of 129 fractures/RA, the total number of fiber fractures at failure would be 3.3×10^5. If each fiber experienced multiple fractures so as to achieve the ineffective length, the total number of fiber fractures in the present example would far exceed this number. It is clear that laminate failure in unidirectional CFRP laminates occurs before such a saturation condition is achieved. Such behavior has been predicted by a number of models [35-37] all of which predicate laminate failure on the achievement of some local critical condition as fiber fractures density and in some way over-stress surviving adjacent fibers. It is not within the scope of the present work to review the various analyses nor to propose a new model. It is however expected that the realization of a sound experimental measure of the load-fiber fracture density relationship for one material system will be of value in this area of continuing analytical activity. Some general observations regarding the relationship of the present results to one of the failure models is presented in a following section.

Some details of the fiber fractures are shown in Figs. 22 and 23. By comparison with previous micrographs of a 0 degree fiber fractures in cross-ply laminates, it is seen that the mode of fiber fracture is indistinguishable. However, the frequency of multiple adjacent fiber

fractures ("multiplets") is generally higher in unidirectional laminates than in cross-ply laminates at the same load even though the number of fiber fractures in the former is lower. Figure 23 shows histograms of multiplet distributions for both unidirectional and cross-ply laminates. Figure 24 presents the same data in terms of strain. Singlets (S) are fiber fractures bounded by two unbroken fibers; a doublet (D) is defined as two adjacent fiber fractures in which the breaks are separated by a distance not greater than five fiber diameters; a triplet (T) is three adjacent fiber fractures in which none of the breaks is separated from an adjacent break by more than five fiber diameters. Quadruplets and higher order multiplets (>4) are defined in a similar way. The choice of five fiber diameters lengthwise separation was arbitrary but was applied uniformly to all specimens. The multiplet distribution was determined at the same time and using the same representative area as that used for the fiber fracture accounting.

The cross-ply multiplet distribution shows a small but consistent shift from singlets to higher order multiplets with increasing load. Even at the highest loads however the multiplet distribution is dominated by singlets, with 11% doublets and less than 1% triplets and higher order multiplets. In fact multiplets of order higher than 4 were not observed in any of the laminates examined. This is not to say that higher order multiplets did not exist, since the counting scheme used was based on representative areas and did not include the entire specimen. However, if laminate failure is predicated upon the development of a "critical multiplet" then the order of this multiplet is likely to be 5-7 for this laminate and material using the authors' definition of a multiplet.

The multiplet distribution for the unidirectional specimens show a similar shift to higher order multiplets. The shift is more pronounced than for the cross-ply laminates such that, at loads near failure, doublets and higher order multiplets represent 20% of the total. At loads above 70% $\overline{S}_{ult}$ there is a marked increase in doublets and higher order multiplets compared to the distribution at loads below this level. The 70% level was seen to be the incipience of substantial fiber fracture in these laminates. These results confirm that weak fibers breaking at low loads have little immediate influence on fracture of adjacent fibers. However when the load approaches the mean fiber strength, the influence of fiber fracture on adjacent fibers becomes significant.

Given the fact that transverse ply cracks should produce elevated stresses in the zone of material adjacent to the crack tip, it is not surprising that the greatest number of fiber fractures occur near these cracks. It is somewhat surprising however that the occurrence of multiplets would be lower in the presence of these cracks than in unidirectional laminates for which there are no cracks. The explanation may lie in the extent of matrix damage produced in the 0 degree plies by adjacent cracks in cross-ply laminates. It has been shown [39] that such cracks produce in the adjacent 0 degree plies tensile stresses transverse to the fiber direction. In fatigue tests of CFRP laminates it has been shown that these stresses are sufficient to produce microcracking parallel to the fiber [28, 33]. Although such microcracks were not observed in X-ray radiographs of the cross-ply laminates in the present series it is possible for such cracks to be quite small, and still have an influence on damage development. Microcracks of this type

would have the effect of isolating fibers and reducing the static and dynamic overstresses from adjacent fiber fractures. To the extent that such a mechanism is not available in unidirectional laminates, the influence of one fiber fracture on adjacent fiber fractures would be greater and the multiplicity of adjacent fractures concomitantly higher. To move this hypothesis beyond conjecture requires the refinement of experimental techniques for examining resin damage in the 10 - 100 mm range.

One final observation is made on the character of the multiple fractures observed in unidirectional specimens. Based upon several thousand observations of fiber fractures in both cross-ply and unidirectional laminates, it appears that unusual patterns of multiplets are more frequently observed in the unidirectional laminates. Some examples are shown in Fig. 25. The appearance of several closely spaced breaks in the same fiber occurs almost exclusively in unidirectional specimens. Given the short lengths of the fiber segments it is likely that fractures of this type occur dynamically. Dynamic mechanisms involving stress wave propagation would be favored for the case of intact interfacial bonds. Such a result is thus consistent with a difference in disbonding between the two cases.

$[0,0]_s$ Acoustic Emission Analysis

Figure 26 shows the cumulative acoustic emission recorded during the tensile loading of a typical $[0,0]_s$ laminate. The occurrence of counts at low loads is attributable to gripping and other spurious noise. The general forms of the event count and count rate versus load relationships are similar to those for non-porous cross-ply specimens.

The point at which both curves deviated from the linear noise line was measured for a number of specimens. The average occurrence of this AE inflection point for the unidirectional specimens was at a load of 49% $\overline{S}_{ult}$. (Data for all specimens are given in Table 3.) That is, some damage begins to occur at this level, but the number of counts is relatively small until the 65-70% $\overline{S}_{ult}$ load level is reached. In the absence of physical evidence of resin damage, this acoustic emission is attributed to isolated fractures of the weakest fibers. At higher loads the cumulative acoustic emission curves take the same form as the cumulative fiber fracture curve.

Figure 27 presents the amplitude distribution data for a typical $[0,0]_s$ specimen. The load levels are the same as previously defined. Events occurring at low load levels are seen to principally populate channels in the range of 4 to 22. In fact for this and all other unidirectional specimens loaded to failure, event amplitudes were generally below channel 25 for all load ranges. The shape of the distributions showed little change with increasing load and no shift to higher amplitudes was observed.

In comparison with the evolution of the amplitude distributions of non-porous cross-ply laminates with increasing load (Figure 17), the results for the unidirectional specimens are seen to be more stationary. Whereas the cross-ply amplitude distribution shifts to higher amplitude channels with increasing load and then retreats slightly to lower channels at loads near failure, the unidirectional specimens can be characterized by a single, low-amplitude-dominated distribution across the load-to-failure spectrum. Such a result is

consistent with the operation of two damage mechanisms in the cross-ply laminate and only one in the unidirectional.

Figure 28 is another representation of the amplitude distribution for this specimen which is typical of many other unidirectional specimens tested. Figure 28a shows the cumulative percentage share of events in various channel ranges as defined previously. The virtual absence of events in channels 22-50 can be seen. Figure 28b is the same analysis with channels 4-9 excluded. It is notable that the fraction of events in channels 16-21 is essentially unchanged through failure. The share of events in channels 10-15 increases at loads near failure. Inasmuch as fiber fractures are the dominant source of acoustic emission near failure, this channel range may best characterize the associated acoustic emission. Figures 29 and 30 show the same data for another unidirectional specimen indicating the repeatability of these results.

The association of fiber fracture with low amplitude acoustic emission is counter to much of the conventional wisdom for acoustic emission in composite materials. Balderston [39] for example has reported much lower discharge of energy from resin cracking near fiber fracture in notched Boron/epoxy laminates. Mullin and Mehan [40] reported similar result for Boron/epoxy between fiber-matrix disbonding and fiber fracture. It is frequently assumed that fiber fracture in any material system will release large amounts of strain energy relative to other damage mechanisms and will therefore be the source of the highest amplitude acoustic emission. This assumption is so common, perhaps because it seems so intuitive, that the lack of substantiating evidence of its general validity is unquestioned.

It is indeed possible that for a particular fiber/resin system and a particular laminate type, fiber fracture may be the source of high amplitude acoustic emission. However, as with nearly all aspects of acoustic emission analyses, the association of an attribute of the acoustic emission pulse, e.g. amplitude, with an attribute of the source of the pulse, e.g. energy, is complicated. First given the dispersive nature of the composite media, there is no assurance that pulses of two different frequencies originating with given relative amplitudes will arrive at the transducer with the same relative amplitudes. Second, fiber fracture occurring in surface plies may yield fundamentally different AE pulses at the receiver than the same fractures occurring in imbedded plies, i.e. the laminate geometry and stacking sequence have an important influence on the characteristics of the received pulse. Third, and perhaps most important in the present context, the average energy released by a particular event is intimately related to the environment in which that event occurs. In the case of fiber fractures for example, it is commonly assumed that because they typically occur at elevated loads, the strain energy released must be greater than for event occurring at lower loads. By invoking this violin string analogy, the reality of fiber fracture is obscured. When fibers which are imbedded in moderately ductile resin matrices break, the strain energy released per unit volume is relatively large

$$\frac{E}{V} = \int_0^{\varepsilon f} \sigma \varepsilon d\varepsilon$$

However the volume of fibers from which this energy is released is quite small if the fiber-matrix near the interface remains in tact away from

the fracture site. It has been shown in woven GRP laminates for example that the energy released by the fracture of a fiber disbonded over a length of 2 mm is approximately 200 times greater than the fracture energy for an undisbonded fracture [12]. The present results for unidirectional CFRP laminates and prior work reported by other investigators [10, 41] indicates that fiber-matrix disbonding in this system is minimal or nonexistent. It would not be expected then that the net energy released by a single fiber fracture, even at loads near failure, should be large.

$[0,90_2]_s$ Porous and $[0,90_2]_s$ Non-porous Laminates

One series of $[0,90_2]_s$ specimens having a high porosity content was characterized and evaluated by acoustic emission monitoring. Results are compared to those for non-porous $[0,90_2]_s$ laminates to assess the influence of material "quality" on damage development and acoustic emission.

Porous $[0,90_2]_s$ Damage Characterization

Figure 31 shows an edge section of a virgin porous $[0,90_2]_s$ specimen. Porosity is seen to exist across all of the 90 degree plies with substantial segregation at the ply interfaces. These interfaces are resin-rich but continuous in the non-porous laminates. In porous specimens, the first crack typically appeared at loads somewhat lower than in non-porous specimens, but the crack density at high loads was equivalent between the two types. The cracks which developed in the porous specimens were noticeably different from those in non-porous specimens. Figure 32 shows an example. The non-porous specimen cracks

are seen in Figure 32a to be essentially self-similar. Cracks in the porous specimens typically appeared as shown in Figure 32b. Cracks tended to follow a more indirect path from interface to interface involving substantially more surface area.

There was an insufficient number of porous $[0,90_2]_s$ specimens to permit a rigorous analysis of crack development rate. However some inference can be drawn from a comparison between the acoustic emission for the porous case with that for the non-porous population for which a more complete damage characterization was possible. This comparison is provided in the following section.

Porous $[0,90_2]_s$ Acoustic Emission Analysis

Figure 33 shows the load versus AE cumulative counts and count rate for a typical porous $[0,90_2]_s$ laminate under tensile loading to failure. The first acoustic emission counts were recorded at approximately 35% $\bar{S}_{ult}$. The count rate increased very rapidly, immediately thereafter then diminished before increasing rapidly again at loads near failure. The result was a characteristic and repeatable "hump" in the cumulative event curve. The average cumulative events at failure on average was identical between the porous and non-porous $[0,90_2]_s$ populations: $2.9 \times 10^4 \pm 2.5 \times 10^4$ counts for the non-porous specimens: $2.9 \times 10^4 \pm 0.4 \times 10^4$ counts for the porous specimens. Data for all specimens are contained in Table 4.

In every test of porous and non-porous $[0,90_2]_s$ laminates this distinctive difference in the structure of the cumulative acoustic emission curve was observed. Incipient acoustic emissions in the porous specimens occurred on average at a lower load level: 36% ± 1% of the

average ultimate stress for porous laminates; 61% ± 10% of the average ultimate stress for the non-porous laminates. The characteristic hump in the AE cumulative event curve was highly repeatable, beginning and ending at virtually identical load levels. Figure 34 presents results from another porous specimen to show the reproducibility of this feature. As a basis for sorting non-porous from porous specimens, this attribute of the acoustic emission alone would have been 100% reliable for the specimens tested.

Figure 35 shows a series of AE event amplitude histograms for the porous $[0,90_2]_s$ laminate of Figure 33. In load range 1 there are more events in higher channels than for non-porous specimens at the same load level. In load range 2, the amplitude distribution has expanded to include events registering in all channels from 4 through 50 with significant numbers of counts in the higher amplitude channels. It should be noted that this is the load interval over which the "hump" in the cumulative count curve occurs and during which the incipience of transverse ply cracks was observed in edge replicas (approximately 35% $\bar{S}_{ult}$ on average for the porous specimens tested).

For load ranges 3 and 4, the high amplitude channels continue to be populated, but the overall amplitude distribution exhibits a marked shift to lower amplitude channels. This trend is seen to be continued in load ranges 5 and 6 so that at loads between 90 and 100 percent of the mean ultimate load, there are few counts above channel 30. Comparing Figures 35 and 17, it is seen that as porous and non-porous specimens approach failure, they produce acoustic emission with comparable maximum amplitudes, but the distribution of amplitudes in the

porous specimens is broader than in the non-porous specimens and includes a relatively larger proportion of events in channels 20 to 30.

Based upon the physical evidence of transverse ply crack formation in porous and non-porous laminates, it is evident that crack formation in porous and non-porous forms of the same resin can be distinguished unambiguously from analysis of the acoustic emission amplitude distributions. The correlation between the occurrence of events in the high amplitude channels in intermediate load ranges and the condition of resin was 100% for the $[0,90_2]_s$ porous and non-porous specimens tested. The distributions of amplitudes in each load range were highly repeatable attributes of the acoustic emission from both populations. Thus acoustic emission amplitude distribution proved to be a very valuable technique for distinguishing between the occurrence of a single damage mechanism, transverse ply cracking, in specimens having different material conditions.

Rationalizing the occurrence of higher amplitude events in the porous specimens is a less certain matter. It is clear from the physical evidence that cracks in porous specimens produce some surfaces which are parallel to the loading direction. Under continued loading, these surfaces can be expected to rub together producing acoustic emissions. Such a mechanism would not be operative in non-porous specimens where the crack surfaces are normal to the load direction and separate under continued loading.

Fiber fracture densities were not recorded for the porous laminates and no correlations can be made between acoustic emission and fiber fracture in this case. If however it is assumed that fiber fracture is associated with high loads then the retreat of the AE amplitude

distribution from high channel ranges at high loads suggest that the high amplitude damage mechanism in these laminates is the development of cracks, not the fracture of fibers. This is fully consistent with the results for the non-porous specimens.

V. Summary and Conclusions

The principal aspects of the present work were damage assessment and acoustic emission analysis. In assessing the damage which occurred in $[0,90_2]_s$ laminates during tensile loading to failure, only transverse ply cracking and fiber fracture were observed. Secondary microdamage such as fiber/matrix disbonding, edge delamination, interior delamination, longitudinal cracking, and longitudinal splitting was not observed even at loads near failure. Such damage has been observed to occur during tension-tension fatigue loading of identical specimens of a similar graphite/epoxy material. Both the crack density and fiber fracture density were shown by direct observation and counting to have a power law type relationship with tensile load. Transverse ply cracks initiate before fiber fractures and serve to localize the subsequent fiber fractures into zones adjacent to the cracks. The same phenomenon has been observed by the present authors for fatigue-damaged laminates. At loads near failure both fiber fractures and transverse ply cracks occur simultaneously.

The only pre-failure damage observed in the $[0,0]_s$ laminate of the same material was fiber fracture. Even at loads near failure, fiber/matrix disbonding, longitudinal cracking or resin microcracking were not observed. The fiber fracture density was shown to have a power law relationship with tensile load similar to that for the $[0,90_2]_s$

laminates. The density of fiber fractures was lower in the unidirectional laminate than in the cross-ply laminate at the same longitudinal strain, reflecting the influence of ply cracks on fiber fractures in the latter. The occurrence of multiple adjacent fiber fractures in the unidirectional specimens was also higher than in the cross ply laminates at the same longitudinal strain suggesting the influence of ply cracks on the mechanisms of load transfer from broken fibers in the two cases.

The amplitude distribution analysis of the acoustic emission recorded during loading exhibited distinct and repeatable structures for the two laminate types. The distinctions were however subtle and were apparent only by detailed analysis and comparison of results from many tests. The unidirectional specimens consistently exhibited lower amplitude acoustic emissions than cross-ply laminates over the load range to failure. Given the physical evidence of damage in these laminates, it is concluded that for this material and stacking sequence fiber fracture is a source of lower amplitude events on average than transverse ply cracking. This conclusion is counter to a widely accepted view that fiber fracture is the source of higher strain energy relative to other recognized damage mechanisms. While this may be true for large fibers such as boron or fiber-resin systems having low interfacial bond strength, the generalization of this hypothesis is fallacious and potentially misleading to the analysis of acoustic emission data in the absence of physical damage assessment.

The power of acoustic emission for discriminating among a population of test pieces on the basis of material quality was demonstrated for porous and non-porous $[0,90_2]_s$ laminates. Both the cumulative AE count and amplitude distributions for the porous specimens

were distinct from the non-porous. Although the total number of counts was the same for the two, the count rates were clearly different and the porous laminates exhibited substantially higher mean amplitudes over certain load ranges than the non-porous laminates. The effectiveness of acoustic emission when used in this way as a screening technique, has been demonstrated for a wide range of materials, structures, and environments, and the current results confirm the value of the technique for this purpose.

The potential role of acoustic emission monitoring in discriminating among damage modes occurring in composite materials is not so clear. In the present work in which the damage modes were very distinctive, evidence of this distinction in the acoustic emission analysis was not remarkable. Not until a substantial body of physical evidence was established and the load-damage relationships were determined explicitly could the AE data be properly interpreted. In the present instance subtle, repeatable differences in the amplitude distribution could be associated with transverse ply cracking and fiber fracture with assurance. Ultimately, however, the validity of the technique must be measured in terms of the potential for generalization of results for special cases such as these to multiaxial laminates in which these damage modes occur in conjunction with others, sometimes simultaneously.

Inference of damage modes and chronology by analysis of the amplitude distribution alone may not be possible in all cases. However the modest success achieved in the present work and the clear promise of acoustic emission as a damage discrimination technique in composite materials strongly suggest that continuing research is warranted.

Acknowledgments

The authors gratefully acknowledge the support of the Defense Advanced Research Project Agency under Contract Number DAAG29-82-K-0190 in the conduct of this research. They also acknowledge the valuable assistance of the following groups and individuals:

- Professor Bryan Harris, Head of the School of Materials Science at the University of Bath, England, for providing facilities, financial support, encouragement, and guidance.
- The faculty and staff of the School of Materials Science for generous assistance in every aspect of the experimental program.
- Dr. Paul Curtis at the Royal Aircraft Establishment, Farnborough, England, for assistance in the fabrication of specimens.
- Mrs. Barbara Wengert at Virginia Tech for typing the manuscript.
- Mr. Peter Ifju for preparing the graphical portions of the report.

Bibliography

1. Williams, R. S. and Reifsnider, K. L., "Investigation of Acoustic Emission During Fatigue Loading of Composite Specimens," J. Composite Materials, Oct. 1974.

2. Duke, J. C., Jr. and Henneke, E. G., "Acoustic Emission Monitoring of Advanced Fiber Reinforced Composite Materials -- A Review," The Fifth International Acoustic Emission Symposium, Tokyo, 1980.

3. Visconti, I. C. and Teti, R., "Acoustic Emission from Composite Materials," NASA TM-75740, March 1980.

4. Guild, E. J., Walton, D., Adams, R. D. and Short, D., "The Application of Acoustic Emission to Fiber-Reinforced Composite Materials," Composites, July 1976.

5. Hamstad, M. A., "Deformation and Failure Information from Composite Materials via Acoustic Emission," VCRL-81272, November 1978.

6. Harris, B., Guild, F. J. and Brown, C. R., "Accumulation of Damage in GRP Laminates," J. Phys. D., Appl. Phys., Vol. 12, 1979.

7. Hamstad, M. A. and Chiao, T. T., "A Physical Mechanism for the Early Acoustic Emission in an Organic-Fiber/Epoxy Pressure Vessel," SAMPE Quarterly, January 1974.

8. Hamstad, M. A. and Chiao, T. T., "Structural Integrity of Fiber/Epoxy Vessels by Acoustic Emission," SAMPE Quarterly, October 1976.

9. Crosbie, G. A., Guild, F. J. and Phillips, M. J., "Acoustic Emission Studies in GRP Composites with Rubber Toughened Matrices," 1st Int'l. Symposium on Acoustic Emission from Reinforced Composites, July 1983.

10. Lorenzo, L. and Hahn, H. T., "Acoustic Emission Study of Fracture of Fibers Embedded in Epoxy Matrix," 1st Int'l. Symposium on Acoustic Emission from Reinforced Composites, July 1983.

11. Fuwa, M., Bunsell, A. R. and Harris, B., "An Evaluation of Acoustic Emission Techniques Applied to Carbon Fiber Composites," J. Phys. D., Appl. Phys., Vol. 9, 1976.

12. Guild, F. J., Phillips, M. G. and Harris, B., "Acoustic Emission Studies of Damage in GRP," NDT International, October 1980.

13. Henneke, E. G., "Signature Analysis of Acoustic Emission from Composites," Final Report, NASA Grant NSG 1238, NASA-CR-145373 (May 1978).

14. Harris, B., "Accumulation of Damage and Non-Destructive Testing of Composite Materials and Structures," Annales de Chimie, June 1979.

15. Phillips, M. G., Ackerman, F. J. and Harris, B., "A Study of Acoustic Emission Amplitude Distributions for Composites, Using Simple Statistical Techniques," Ultrasonics International, 1981.

16. Phillips, M. G., Guild, F. J., Ackerman, F. J. and Harris, B., "Acoustic Emission Monitoring of RP Materials and Pressurized Model Components for Process Plant," 37th Annual Conference, Reinforced Plastics/Composites Institute, Society of the Plastics Industry, January 1982.

17. Guild, F. J., Ackerman, F. J., Phillips, M. G. and Harris, B., "Amplitude Distribution Analysis of Acoustic Emission from Composites: The Development of a Data Collection and Processing System," 1st Int'l. Symposium on Acoustic Emission from Reinforced Composites, The Society of the Plastics Industry, July 1983.

18. Graham, L. J., "Acoustic Emission Signal Analysis for Failure Mode Identification," ASNT Spring Conference, March 1980.

19. Becht, J., Schwalbe, H. J. and Eisenblather, J., Composites, July 1976.

20. Awerbach, J., "Monitoring Damage Progression in CFRP by Acoustic Emission," Schaderismechanik van faserverstärkten verbundstrukturen, DFVLR-Mitt 81-25, October 1981 (in English).

21. Block, J., "Monitoring of Defect Progression by Acoustic Emission," AGARD Meeting, London, April 1983.

22. Reifsnider, K. L., "Mechanics of Failure of Composite Materials," Fracture Mechanics Symposium on Naval Structural Mechanics, September 1978.

23. Wang, A. S. D., "Fracture Mechanics of Sublaminate Cracks," AGARD Meeting, London, April 1983.

24. Bader, M. G., Bailey, J. E., Curtis, P. T. and Parvizi, A., "The Mechanisms of Initiation and Development of Damage in Multi-Axial Fiber-Reinforced Plastic Laminates," ICM3, Vol. 3, August 1979.

25. Korczynskyj, J. and Morley, J. G., "Constrained Cracking in Cross-Ply Laminates," Journal of Materials Science 16, 1981.

26. Harris, B., "Micromechanisms of Crack Extension in Composites," Metal Science, August 1980.

27. Rosen, B. W., "Tensile Failure of Fibrous Composites," AIAA Journal, November 1964.

28. Reifsnider, K. L. and Jamison, R. D., "Fracture of Fatigue-Loaded Composite Laminates," Int'l. Journal of Fatigue, April 1982.

29. Freeman, S. M., "Characterization of Lamina and Interlaminar Damage in Graphite-Epoxy Composites by the Deply Technique," ASTM STP 787, 1982.

30. O'Brien, T. K., "Characterization of Delamination Onset and Growth in a Composite Laminate," ASTM STP 787, 1982.

31. Stalnaker, D. O. and Stinchcomb, W. W., "Load History-Edge Damage Studies in Two Quasi-Isotropic Graphite-Epoxy Laminates," ASTM STP 674, 1979.

32. Masters, J. E., "An Experimental Investigation of Cumulative Damage Development in Graphite Epoxy Laminates," PhD Dissertation, Virginia Polytechnic Institute and State University, March 1981.

33. Jamison, R. D., Schulte, K., Reifsnider, K. L. and Stinchcomb, W. W., "Characterization and Analysis of Damage Mechanisms in Tension-Tension Fatigue of Graphite Epoxy Laminates," ASTM Conference on the Effects of Defects in Composites, San Francisco, December 1982.

34. Zweben, C. and Rosen, B. W., "Statistical Theory of Material Strength with Application to Composite Materials," J. of the Mechanics and Physics of Solids, Vol. 18, 1970.

35. Tamuzs, V., "Dispersed Fracture of Unidirectional Laminates," Fracture of Composite Materials, G. Sih, Ed., 1978.

36. Batdorf, S. B., "Tensile Strength of Unidirectionally Reinforced Composites -- I," J. of Reinforced Plastics and Composites, 1982.

37. O'Brien, T. K. and Reifsnider, K. L., "Fatigue Damage Evaluation Through Stiffness Measurements in Boron Epoxy Laminates," J. of Composite Materials, January 1981.

38. Reifsnider, K. L. and Talug, A., "Analysis of Stress Fields in Composite Laminates with Interior Cracks," VPI-E-78-23, September 1978.

39. Balderston, H. L., "The Broad Range Detection of Incipient Failure Using the Acoustic Emission Phenomena," ASTM STP 505, 1972.

40. Mehan, R. L. and Mullin, J. V., "Analysis of Composite Fracture Mechanisms Using Acoustic Emissions," J. Composite Materials, 5, 1971.

41. Fuwa, M., Bunsell, A. R. and Harris, B., "Acoustic Emission and Fatigue of Reinforced Plastics," Composites -- Standards, Testing and Design.

42. Jamison, R. D., "Advanced Fatigue Damage in Graphite/Epoxy Laminates," PhD Dissertation, Virginia Polytechnic Institute and State University, Aug. 1982.

43. Reifsnider, K. L., Henneke, E. G. and Stinchcomb, W. W., "Defect-Property Relationships in Composite Materials," Proceedings, 14th Annual Society of Engineering Science Meeting, Lehigh University, Bethlehem, PA, 14-16 Nov. 1977.

44. Reifsnider, K. L., "Some Fundamental Aspects of the Fatigue and Fracture Response of Composite Materials," Proceedings, 14th Annual Meeting, Society of Engineering Science Meeting, Lehigh University, 1977.

45. Reifsnider, K. L. and Highsmith, A. L., "Characteristic Damage States: A New Approach to Representing Fatigue Damage in Composite Laminates," Materials: Experimentation and Design in Fatigue (Westbury House, Guildford, England), 1981.

Table 1

Mechanical Properties and Specifications

Material: T300/Code 91
Source: Fothergill and Harvey

	$[0,90_2]_s$ Porous	$[0,90_2]$ Non-Porous	$[0_2]$ Non-Porous
Average ply thickness	0.157 mm	0.153 mm	0.160 mm
Fiber volume fraction	0.620	0.630	0.611
Percent voids	3.9	(1)	(1)
Average ultimate stress $\bar{S}_{ult}$	494±14MPa	550±17MPa	1445±89MPa
Average ultimate strain $(\bar{\varepsilon}_{ult})$	(2)	1.19±0.04%	1.12±0.07%
Average longitudinal stiffness $(\bar{E}_x)$	(2)	43.9±2.5GPA	126±4GPa
Number of specimens represented	6	6	6

(1) Not measurable

(2) No data

Table 2. Summary of Fiber Fracture Density Measurements.

Specimen	Type	Strain (%)	Load (% $\bar{S}_{ult}$)	No. of measure-ments	Fiber fracture density	Multiplicity S	D	T	> 4
IV-J-2-1	$[0,90_2]_s$	0	0	7	10±5	98	1	1	0
IV-J-2-13	$[0,90_2]_s$	0.35	30	10	16±5	98	1	1	0
IV-J-2-27	$[0,90_2]_s$	0.80	70	12	12±5	99	<1	1	1
IV-J-2-15	$[0,90_2]_s$	1.04	86	12	41±24	94	5	<1	0
IV-J-2-28	$[0,90_2]_s$	1.15	90	12	54±32	91	8	1	<1
IV-J-2-10	$[0,90_2]_s$	ND	100	14	107±29	91	8	1	<1
IV-J-2-16	$[0,90_2]_s$	1.26	102	8	129±32	88	11	<1	<1
IV-B-1-1	$[0,0]_s$	0	0	3	10±2	100	0	0	0
IV-B-1-6	$[0,0]_s$	0.36	30	6	12±7	84	5	9	9
IV-B-1-13	$[0,0]_s$	0.54	50	9	13±5	96	4	0	0
IV-B-1-7	$[0,0]_s$	0.80	70	16	16±11	86	13	1	<1
IV-B-1-14	$[0,0]_s$	1.07	85	12	20±7	80	17	3	0
IV-B-1-7	$[0,0]_s$	1.02	96	14	28±12	85	13	2	0
IV-B-1-23	$[0,0]_s$	1.19	100	14	38±18	79	20	<1	<1
IV-B-1-18	$[0,0]_s$	1.15	102	18	29±13	85	13	2	<1
IV-B-1-22	$[0,0]_s$	1.20	103	11	52±15	80	16	3	1

Table 3. Summary of Acoustic Emission Data

Specimen	Type	AE Inflection Point LOAD (kN)	AE Inflection Point % S_{ult}
IV-J-1-1	$[0,90_2]_s$ Porous	4.4	37
IV-J-1-2	"	4.1	35
IV-J-1-4	"	4.0	35
		4.2±0.2	36±1
IV-J-2-3	$[0,90_2]_s$ Non-porous	6.1	47
IV-J-2-4	"	7.3	54
IV-J-2-5	"	7.2	56
IV-J-2-15	"	6.7	51
IV-J-2-16	"	6.8	51
IV-J-2-17	"	6.7	51
IV-J-2-18	"	7.6	59
IV-J-2-19	"	5.6	44
IV-J-2-20	"	6.6	50
IV-J-2-21	"	5.5	44
IV-J-2-22	"	7.1	59
IV-J-2-23	"	6.9	52
IV-J-2-28	"	7.5	57
		6.7±0.7	52±5
IV-B-1-2	$[0,0]_s$ Non-porous	13.3	57
IV-B-1-4	"	9.4	46
IV-B-1-5	"	12.7	53
IV-B-1-7	"	10.7	47
IV-B-1-8	"	10.7	47
IV-B-1-9	"	12.5	53
IV-B-1-10	"	11.6	48
IV-B-1-11	"	13.2	58
IV-B-1-12	"	11.5	51
IV-B-1-14	"	11.0	47
IV-B-1-15	"	9.5	45
IV-B-1-16	"	10.9	44
IV-B-1-18	"	12.5	54
IV-B-1-19	"	11.6	49
IV-B-1-20	"	9.9	43
		11.4±1.3	49±5

S_{ult} = measured laminate strength.

Table 4. Summary of Failure Data

Specimen	Type	Stress (MPa)	$\frac{\%}{S_{ult}}$	Strain (%)	$\frac{\%}{S_{ult}}$	Cumulative AE (10^4 counts)
IV-J-1-1	$[0,90_2]_s$ Porous	536	103	ND	ND	2.9
IV-J-1-2	"	524	101	ND	ND	2.6
IV-J-1-4	"	500	96	ND	ND	3.3
		520±8				2.9±0.4
IV-J-2-3	$[0,90_2]_s$ Non-porous	543	99	1.90	101	4.8
IV-J-2-4	"	573	104	ND	ND	5.0
IV-J-2-5	"	548	100	ND	ND	3.0
IV-J-2-8	"	559	100	1.27	107	3.8
IV-J-2-18	"	547	99	1.16	97	1.3
IV-J-2-19	"	531	97	1.20	101	1.7
IV-J-2-21	"	541	98	1.23	103	1.6
IV-J-2-22	"	525	95	1.14	96	1.8
		545		1.20±0.05		2.9±1.5
IV-B-1-2	$[0,0]_s$ Non-porous	1501	104	1.15	103	2.0
IV-B-1-4	"	1248	86	0.99	88	0.7
IV-B-1-5	"	1476	102	1.19	106	0.7
IV-B-1-9	"	1480	102	ND	ND	2.6
IV-B-1-10	"	1516	105	1.18	105	2.7
IV-B-1-11	"	1377	95	ND	ND	1.1
IV-B-1-12	"	1355	94	0.98	88	2.7
IV-B-1-16	"	1549	107	1.19	106	1.5
IV-B-1-17	"	1470	102	1.18	105	1.2
IV-B-1-19	"	1440	100	1.09	97	2.6
IV-B-1-20	"	1420	98	1.11	99	1.3
IV-B-1-21	"	1564	108	1.13	101	2.7
		1445±86		1.12±0.07		1.8±0.8

ND = No data.

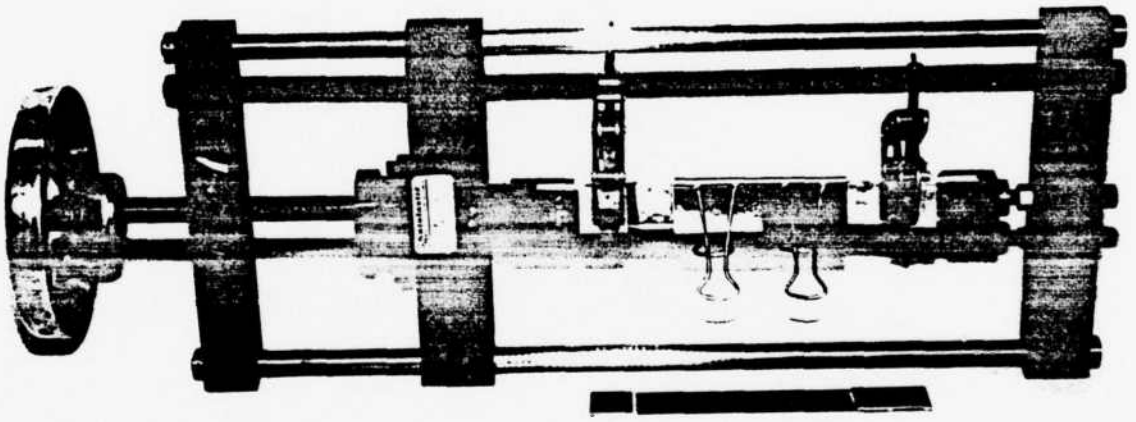

Fig. 1. Loading fixture for the application of X-ray enhancing penetrant.

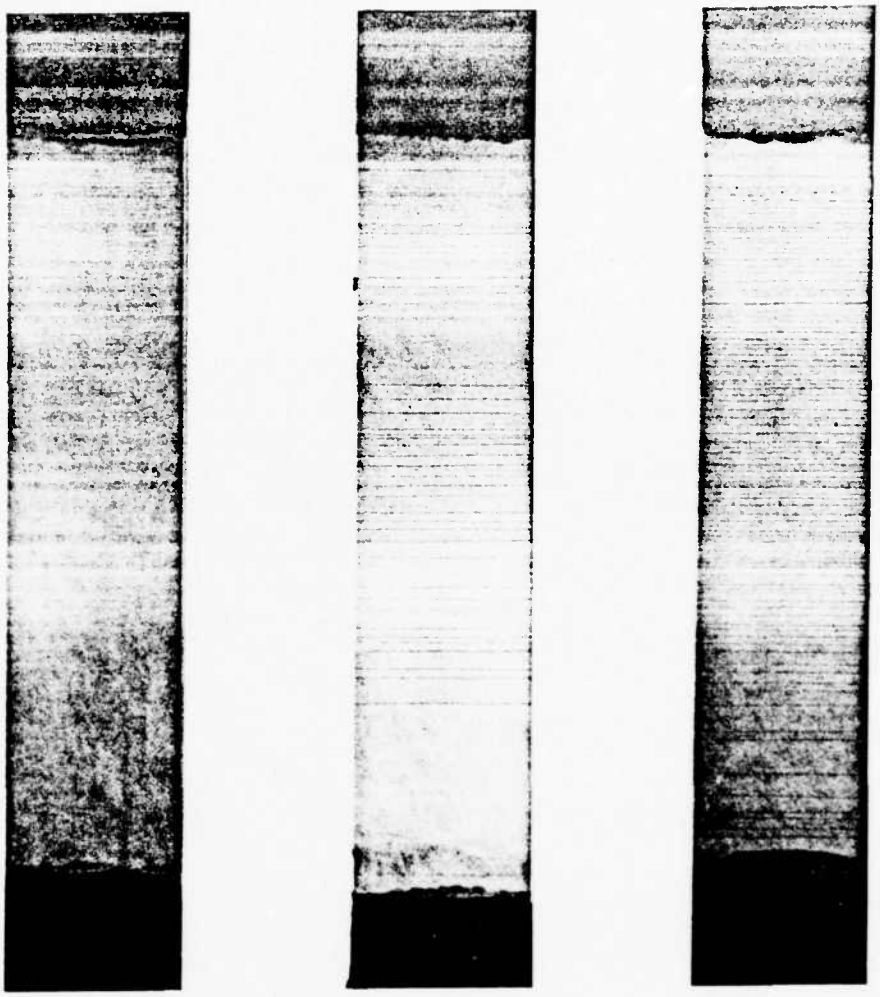

30% $\bar{S}_{ULT}$ a

70% $\bar{S}_{ULT}$ b

100% $\bar{S}_{ULT}$ c

Fig. 2. X-ray radiographs of $[0,90_2]_s$ laminates at tensile loads of (a) 30% $\bar{S}_{ult}$, (b) 70% $\bar{S}_{ult}$ and (c) 100% $\bar{S}_{ult}$.

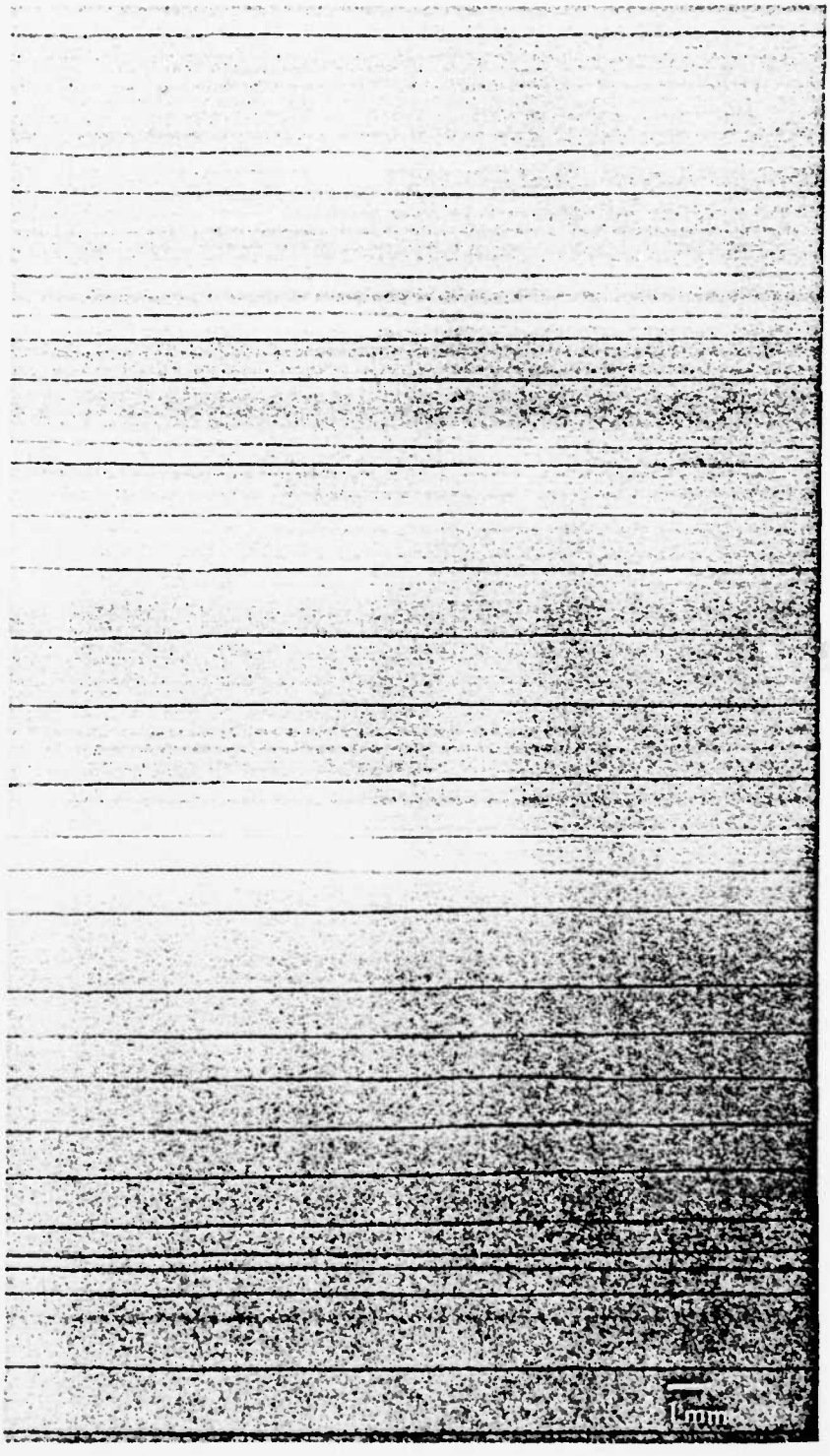

Fig. 3. Detail of Fig. 2 (b) showing transverse ply cracks.

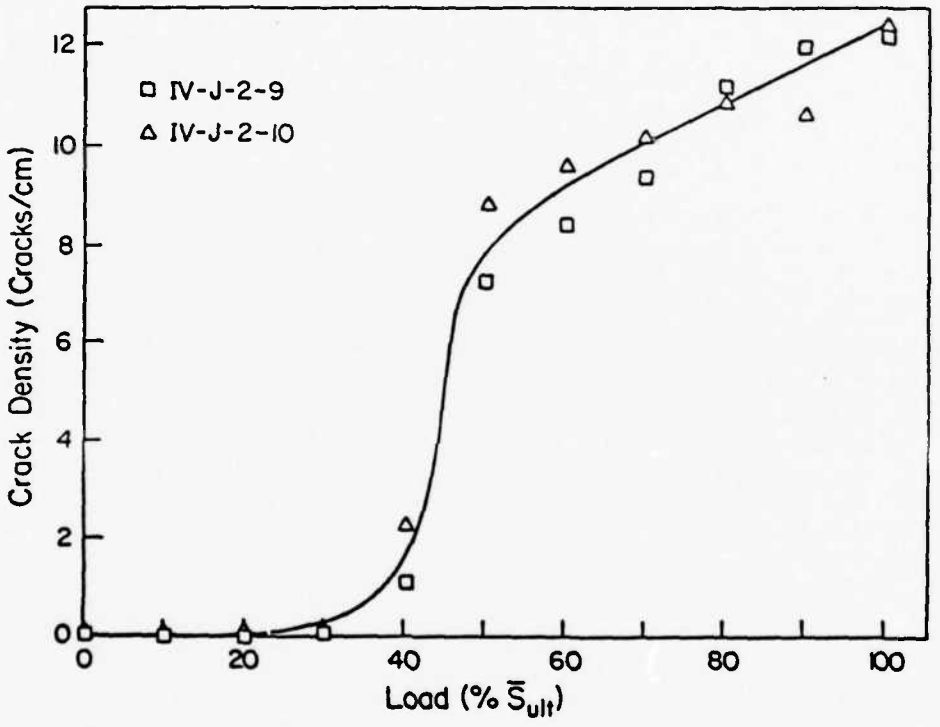

Fig. 4. Crack density vs. load for non-porous $[0,90_2]_s$ laminates.

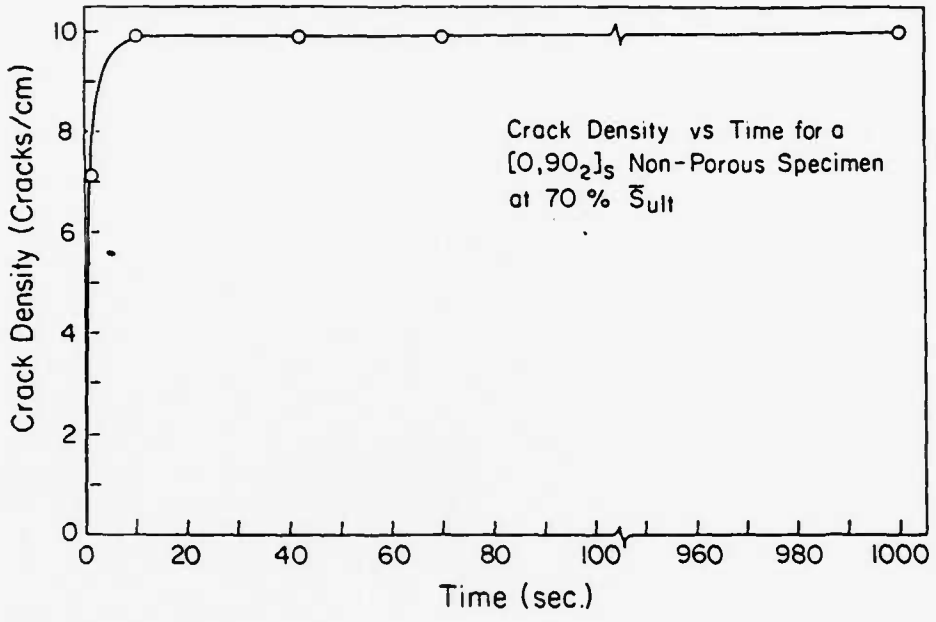

Fig. 5. Crack density vs. time for a $[0,90_2]_s$ laminate at a sustained tensile load of 70% $\bar{S}_{ult}$.

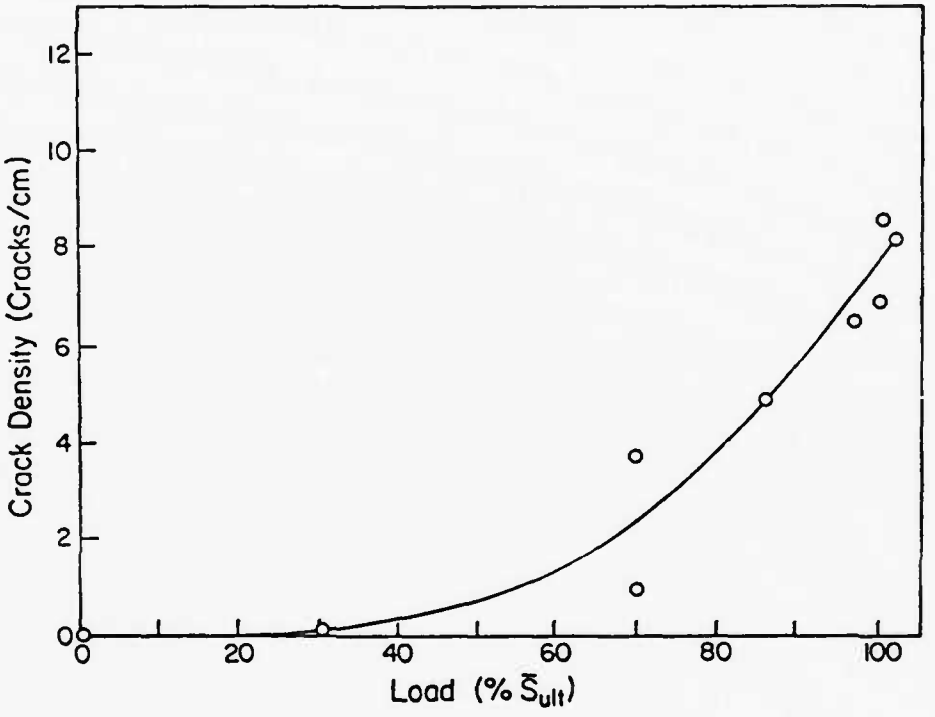

Fig. 6. Crack density vs. load for non-porous $[0,90_2]_s$ laminates.

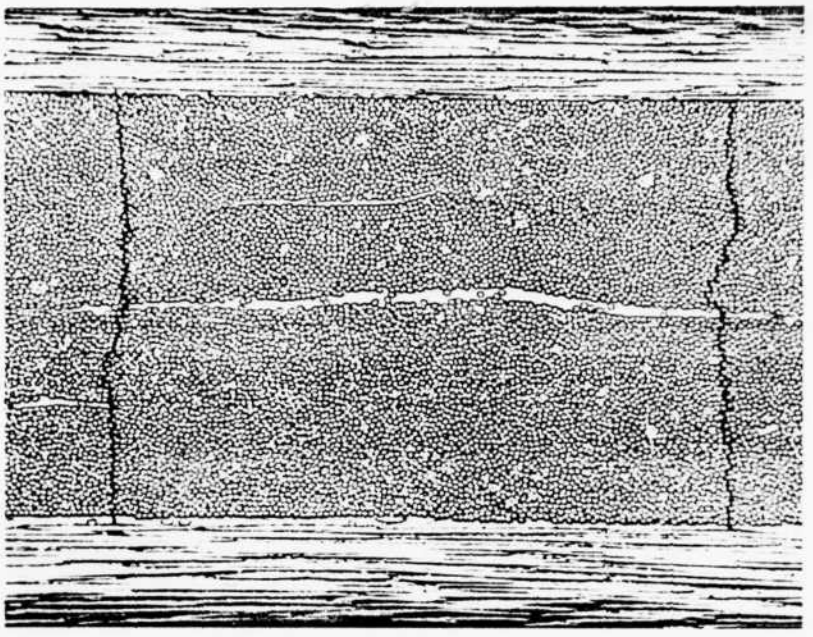

a

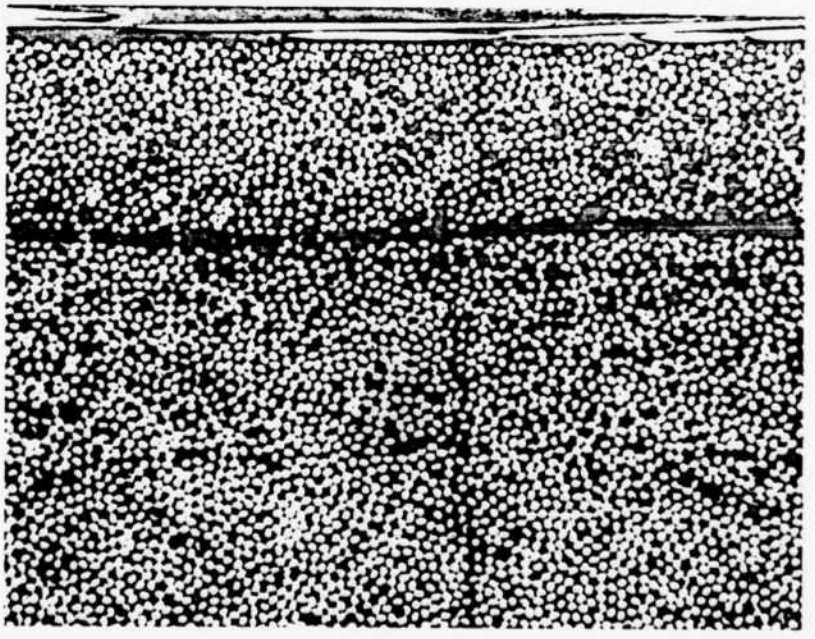

b

Fig. 7. Details of transverse ply cracks in non-porous $[0,90_2]_s$ laminates.

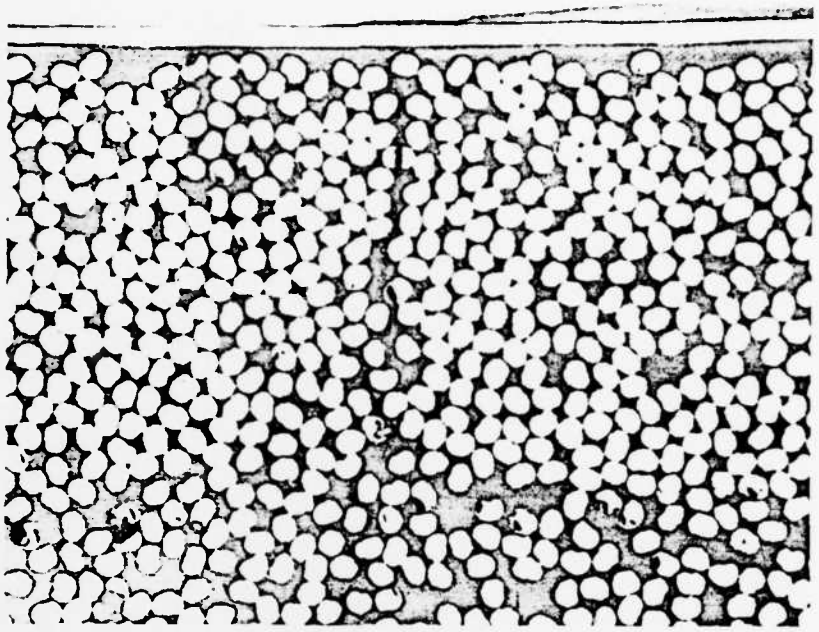

c

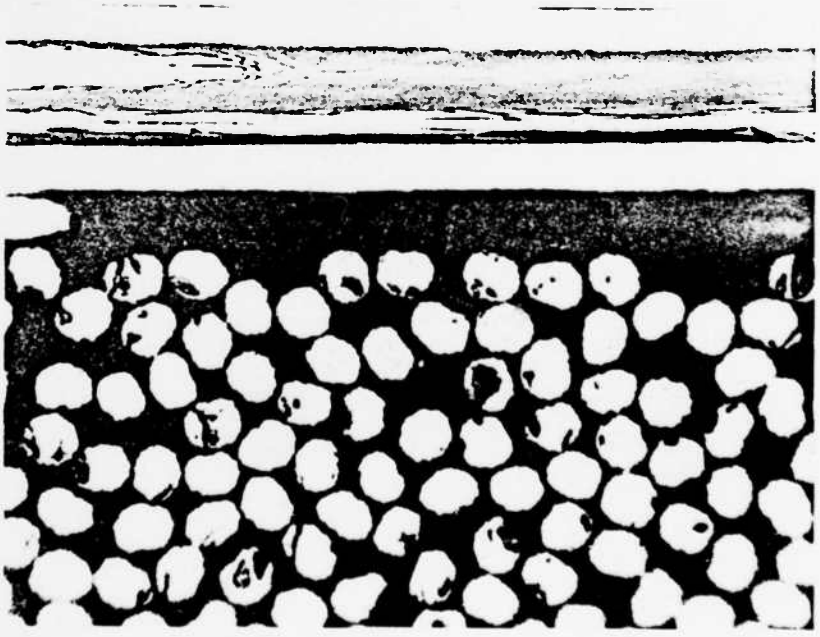

d

Fig. 7. (continued) Details of transverse ply cracks in non-porous $[0,90_2]_s$ laminates.

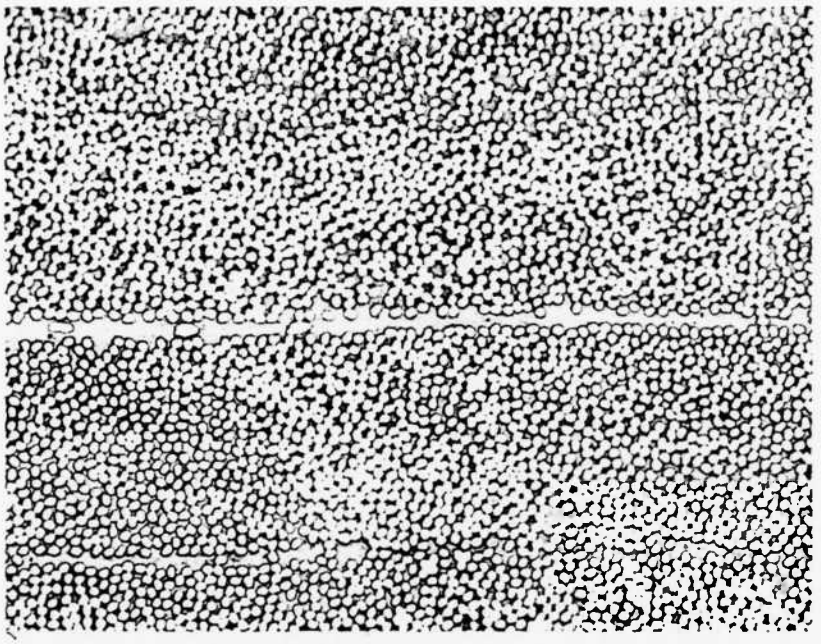

a

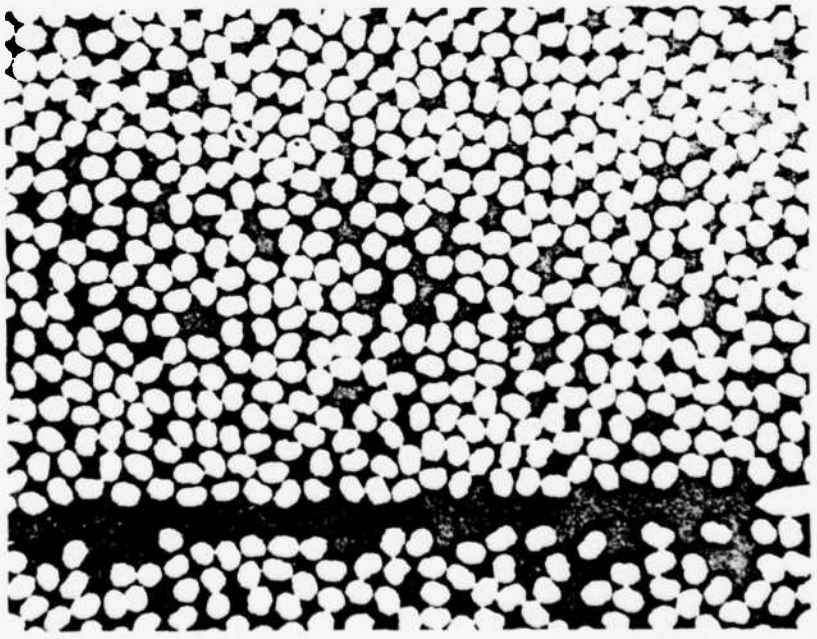

b

Fig. 8. Details of the edge section of a virgin non-porous $[0,90_2]_s$ laminate showing the 90 degree plies.

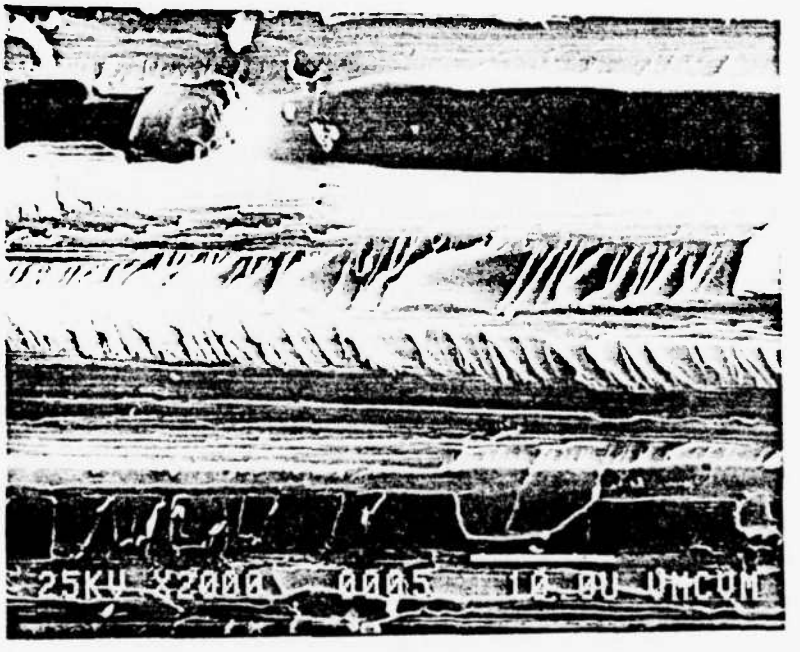

Fig. 9. Surface of a transverse ply crack in a non-porous $[0,90_2]_s$ laminate.

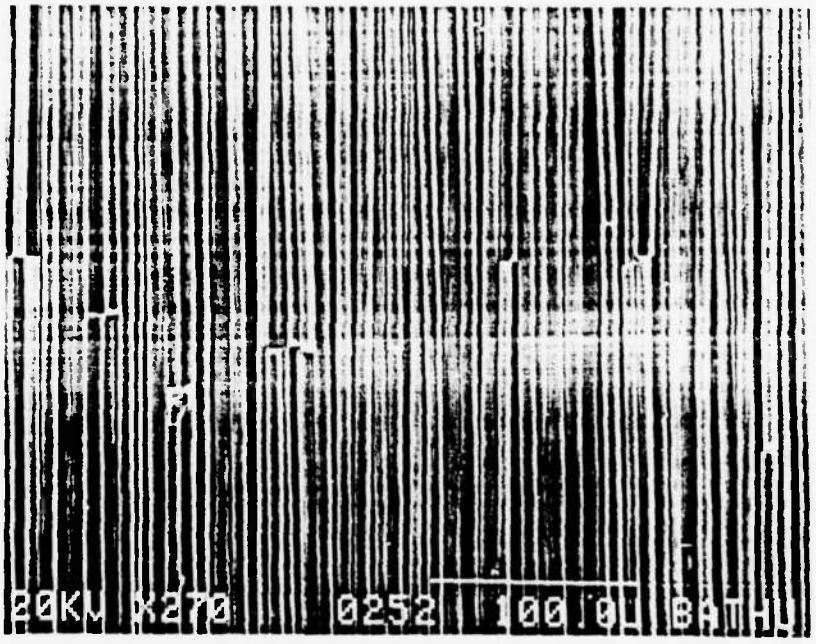

Fig. 10. Fiber fracture pattern in a 0 degree ply from a $[0,90_2]_s$ laminate.

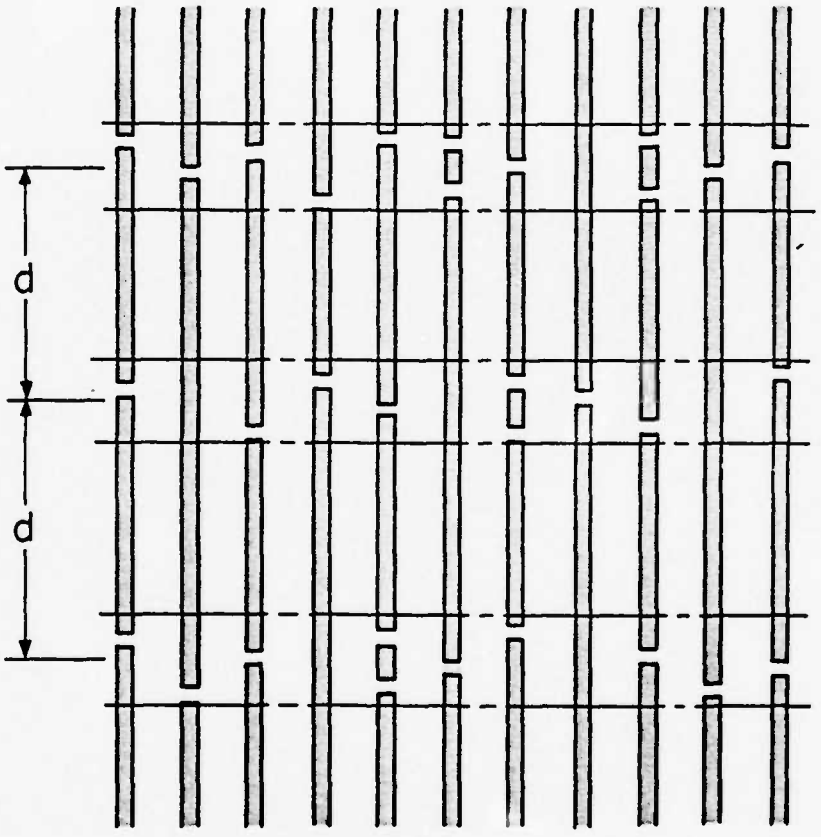

Fig. 11. Schematic of the fiber fracture pattern observed in tensile loading of $[0,90_2]_s$ laminates.

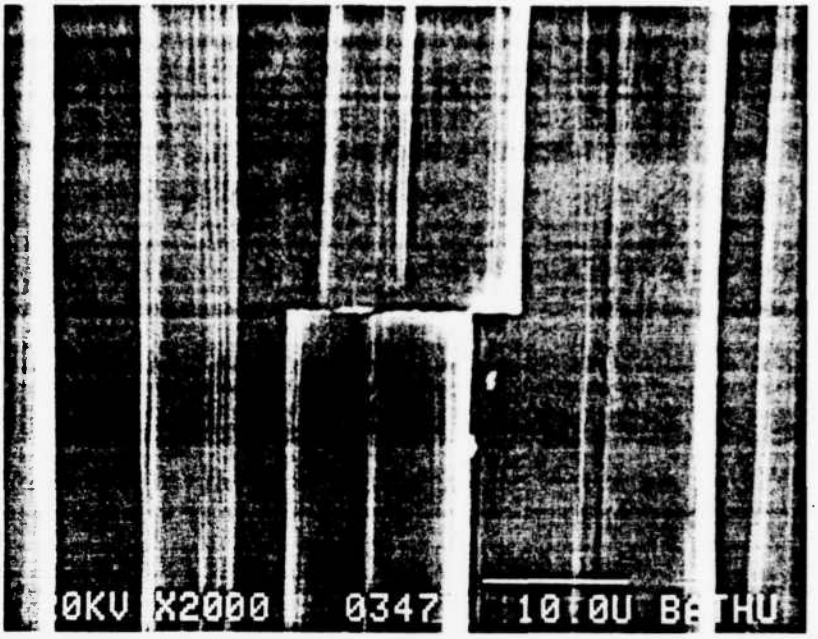

a

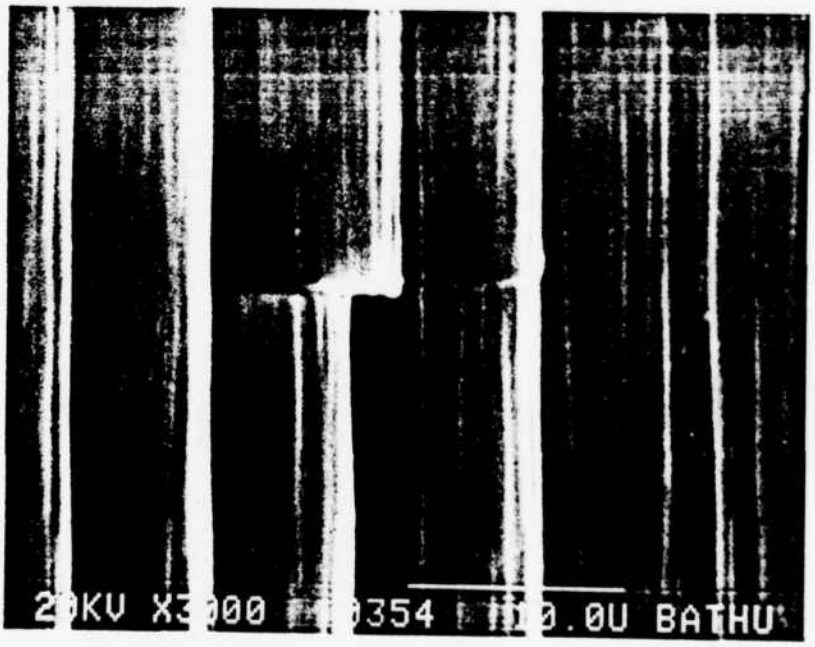

b

Fig. 12. Details of fiber fractures in $[0,90_2]_s$ laminates.

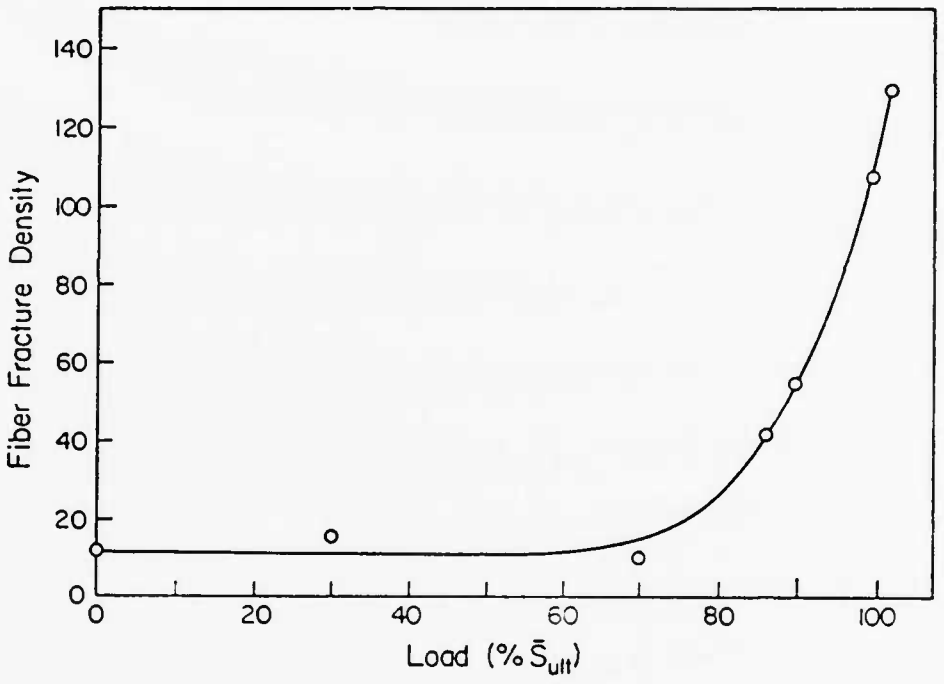

Fig. 13. Fiber fracture density vs. load for non-porous $[0,90_2]_s$ laminates.

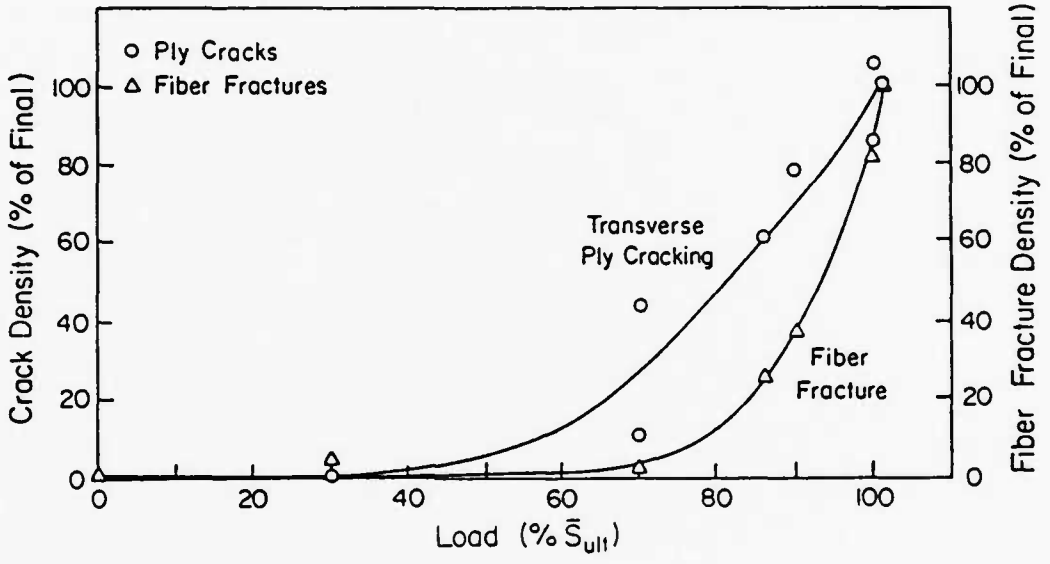

Fig. 14. Normalized transverse ply crack density and fiber fracture density vs. load for non-porous $[0,90_2]_s$ laminates.

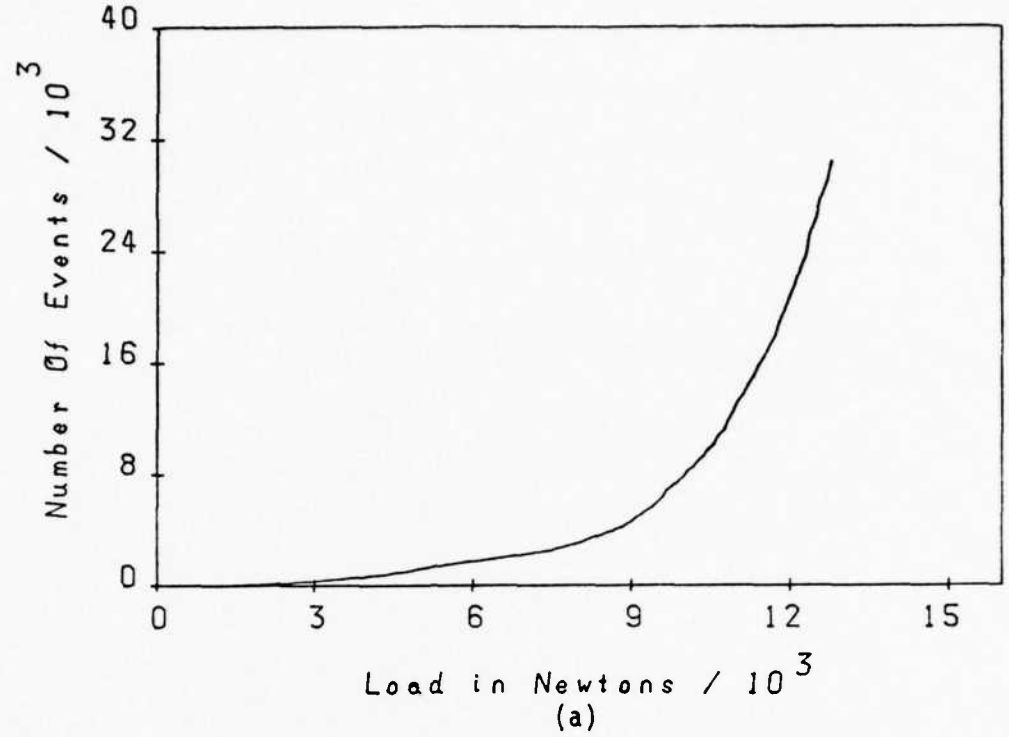

(a)

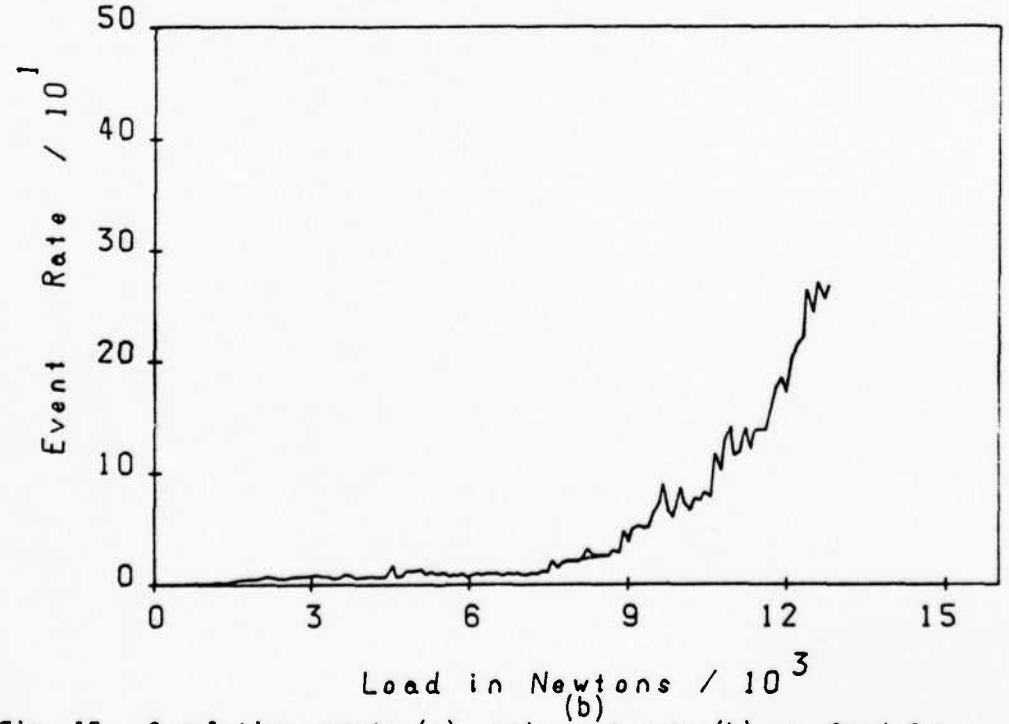

(b)

Fig. 15. Cumulative events (a) and event rate (b) vs. load for a non-porous $[0,90_2]_s$ laminate.

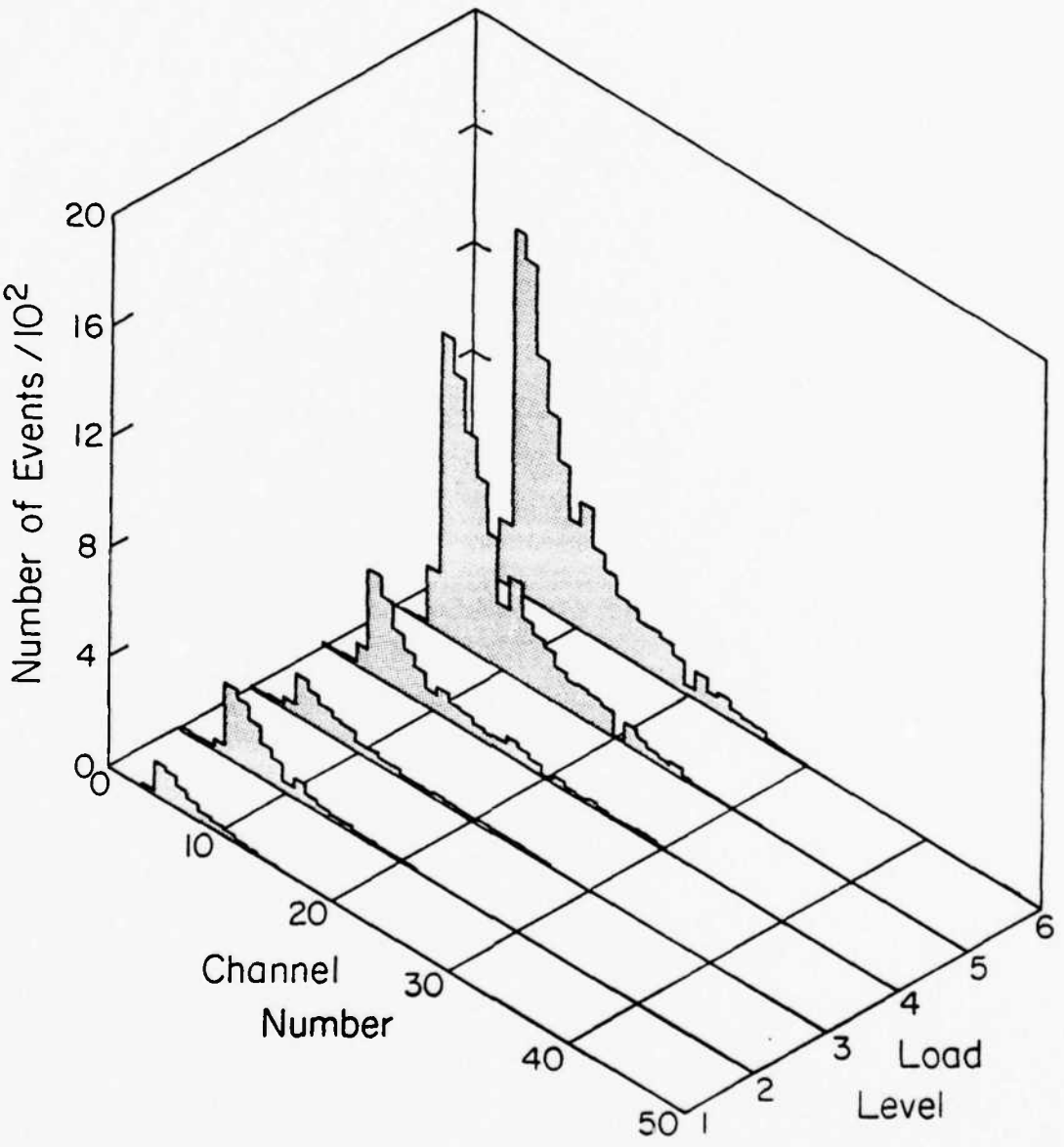

Fig. 16. Amplitude distributions by load level for a non-porous $[0,90_2]_s$ laminate.

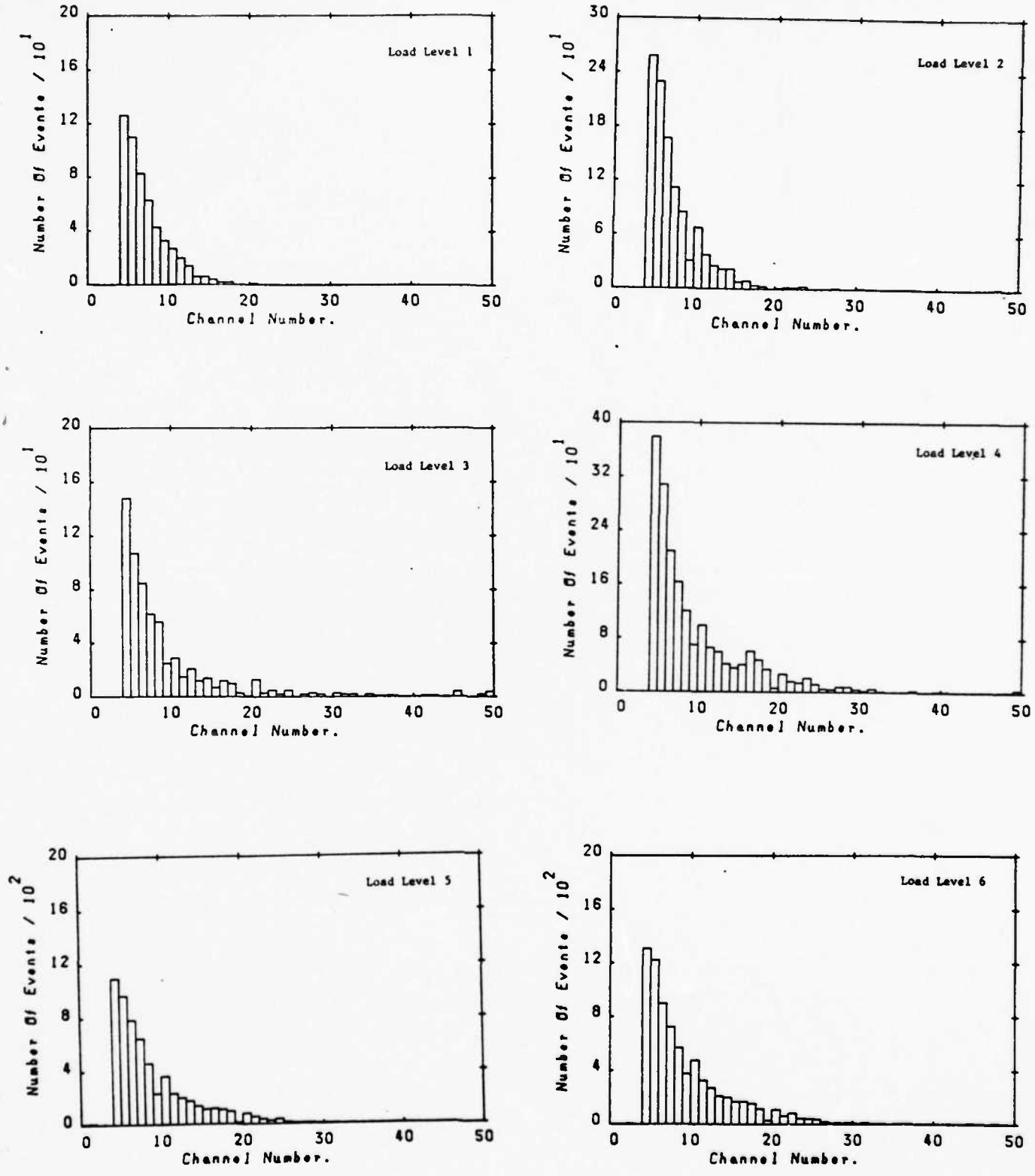

Fig. 16. (continued) Amplitude distributions by load level for a non-porous $[0,90_2]_s$ laminate.

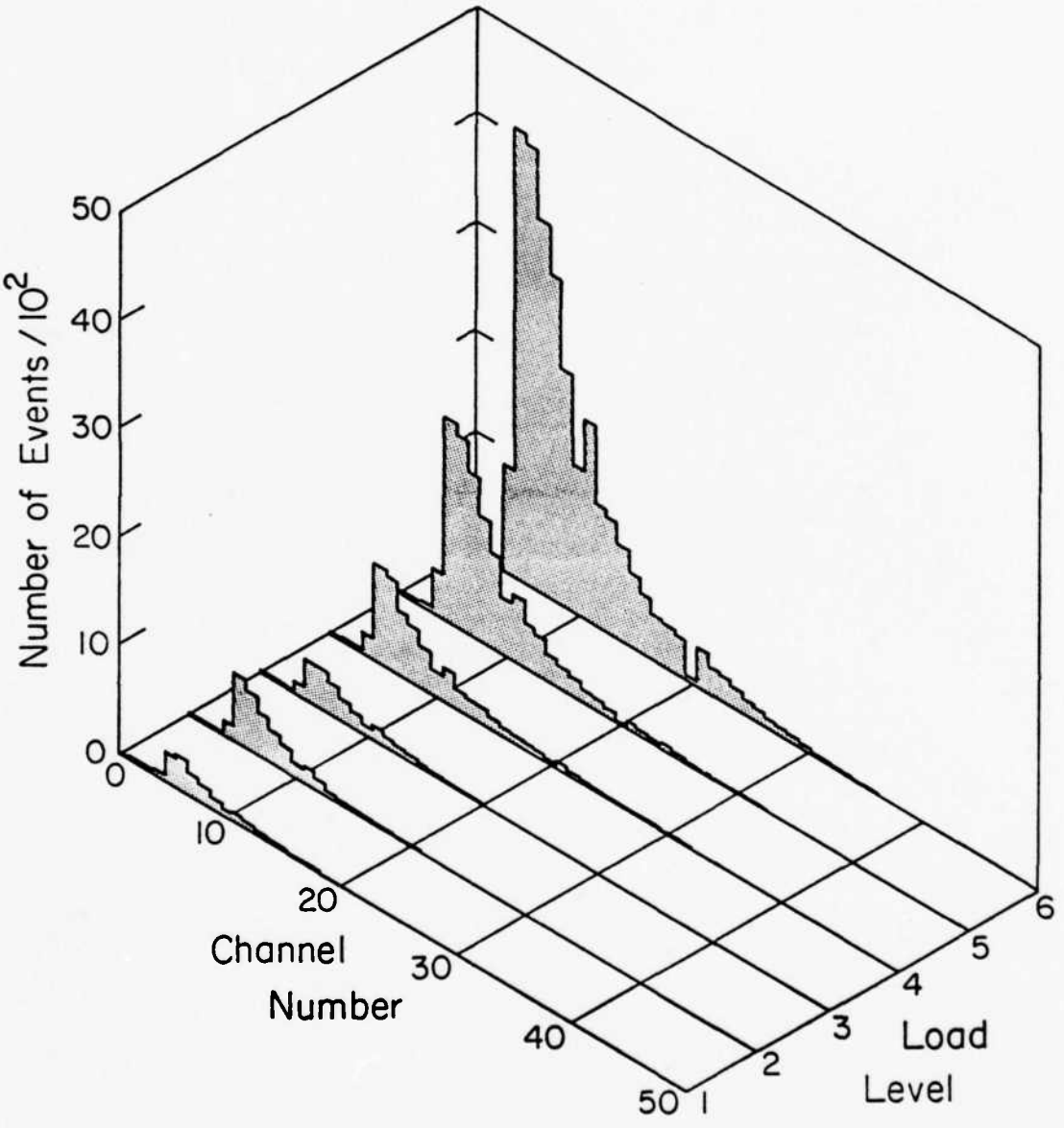

Fig. 17. Amplitude distributions by load level for a non-porous $[0,90_2]_s$ laminate.

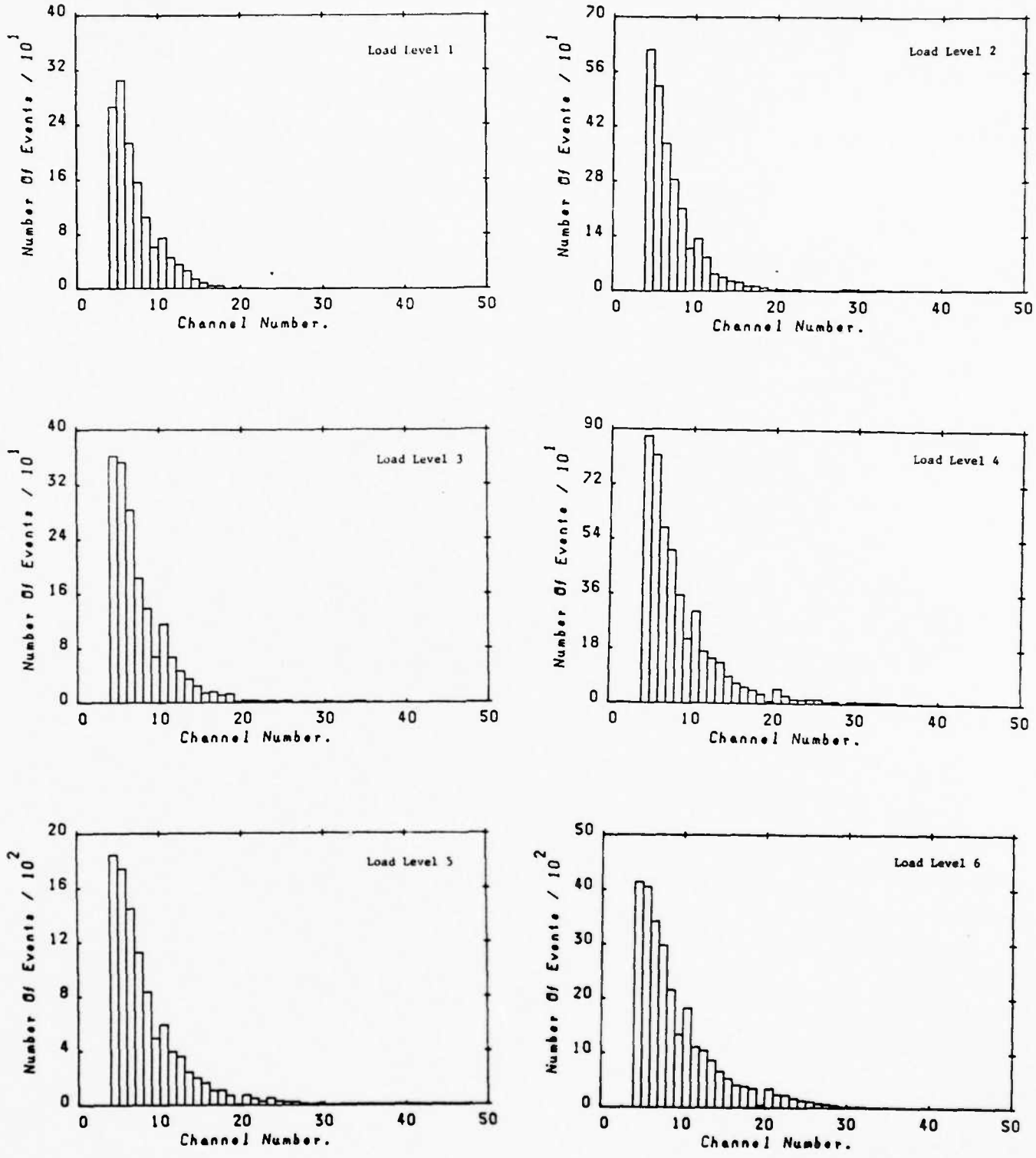

Fig. 17. (continued) Amplitude distributions by load level for a non-porous $[0,90_2]_s$ laminate.

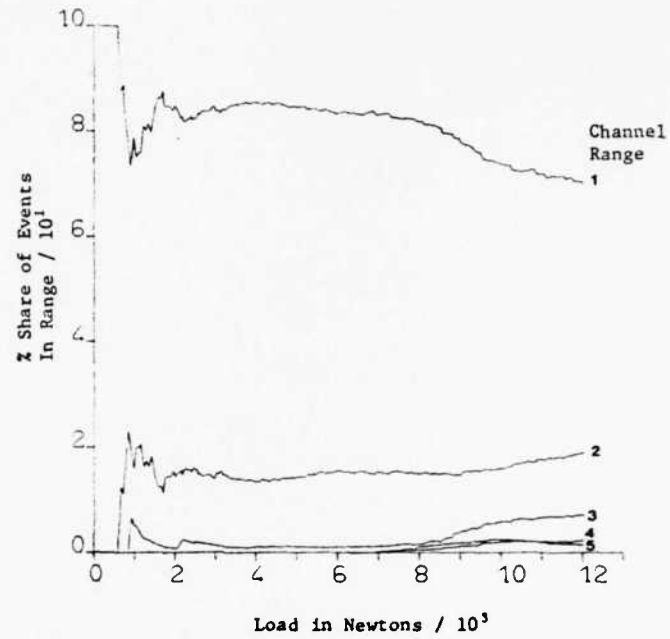

(a)

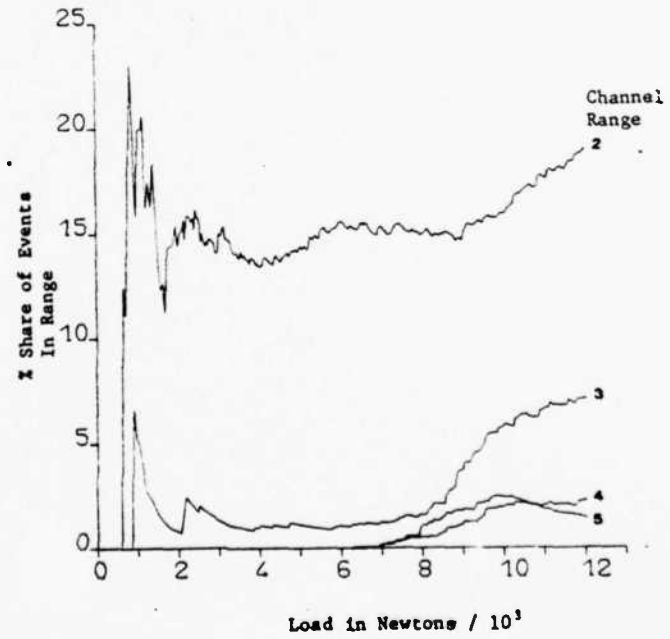

(b)

Fig. 18. Percent share of events in range vs. load for a non-porous $[0,90_2]_s$ laminate. (a) *Including channel range 1*; (b) excluding channel range 1.

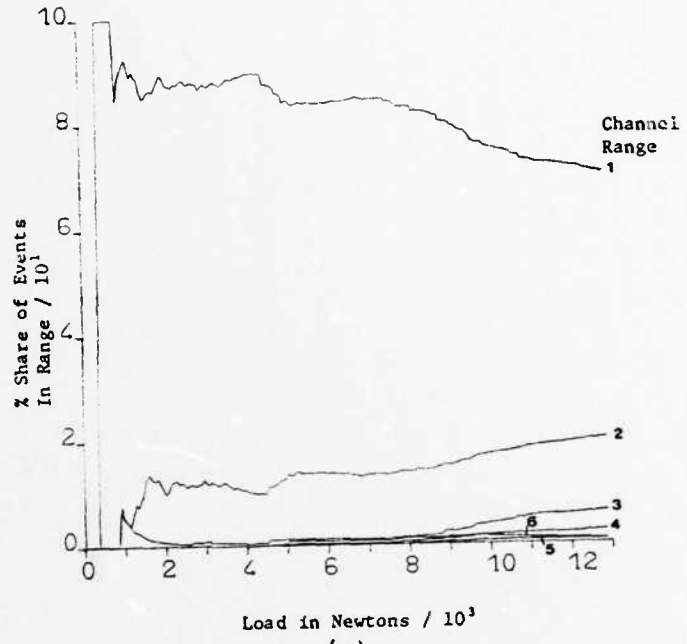

(a)

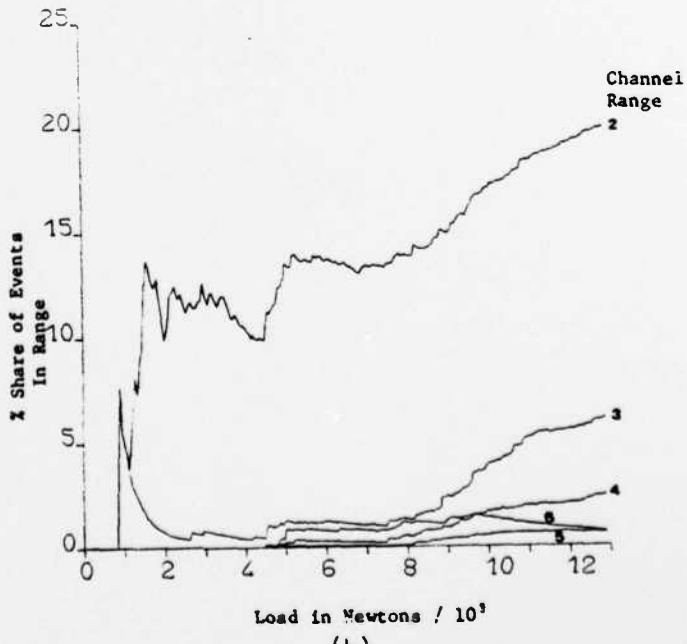

(b)

Fig. 19. Percent share of events in range vs. load for a non-porous $[0,90_2]_s$ laminate. (a) Including channel range 1; (b) excluding channel range 1.

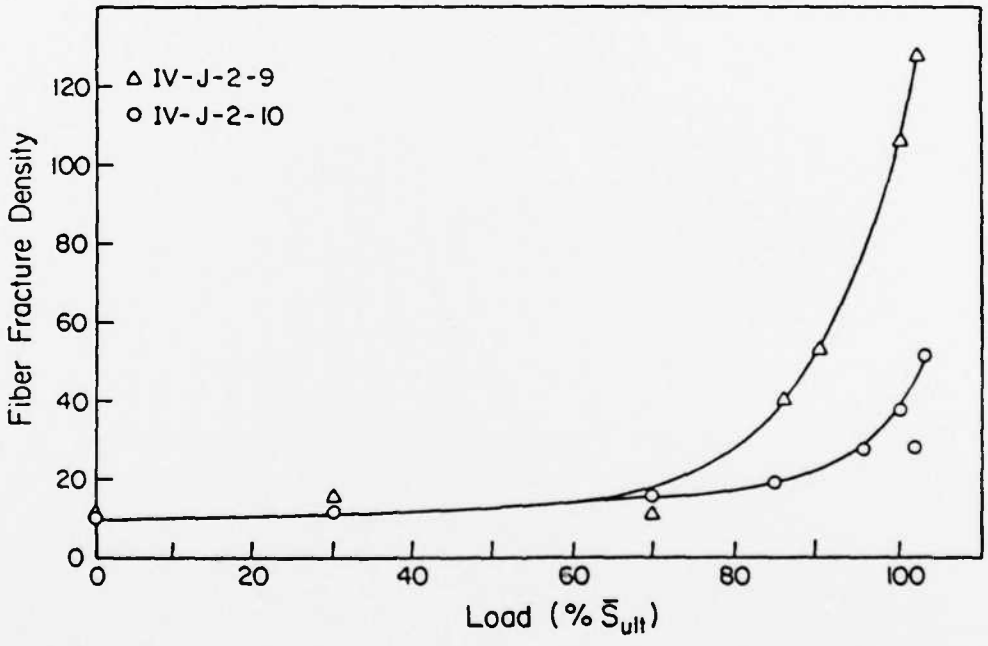

Fig. 20. Fiber fracture density vs. load for non-porous $[0,90_2]_s$ and $[0,0]_s$ laminates.

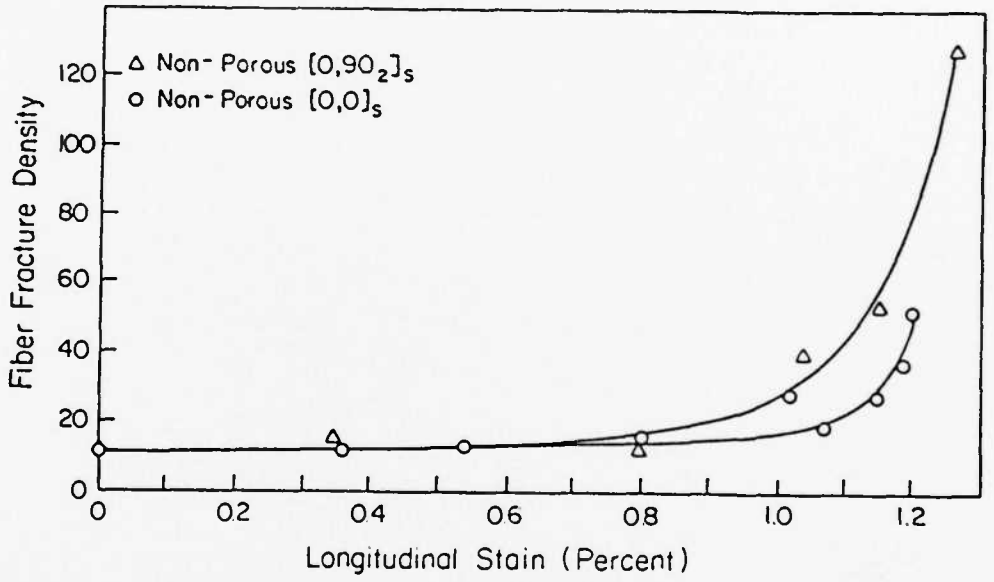

Fig. 21. Fiber fracture density vs. longitudinal strain for non-porous $[0,90_2]_s$ and $[0,0]_s$ laminates.

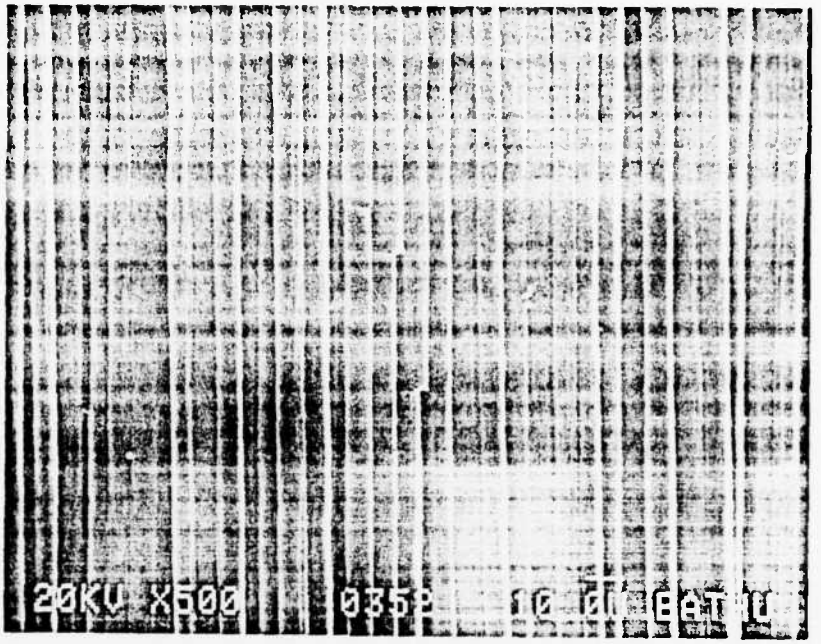

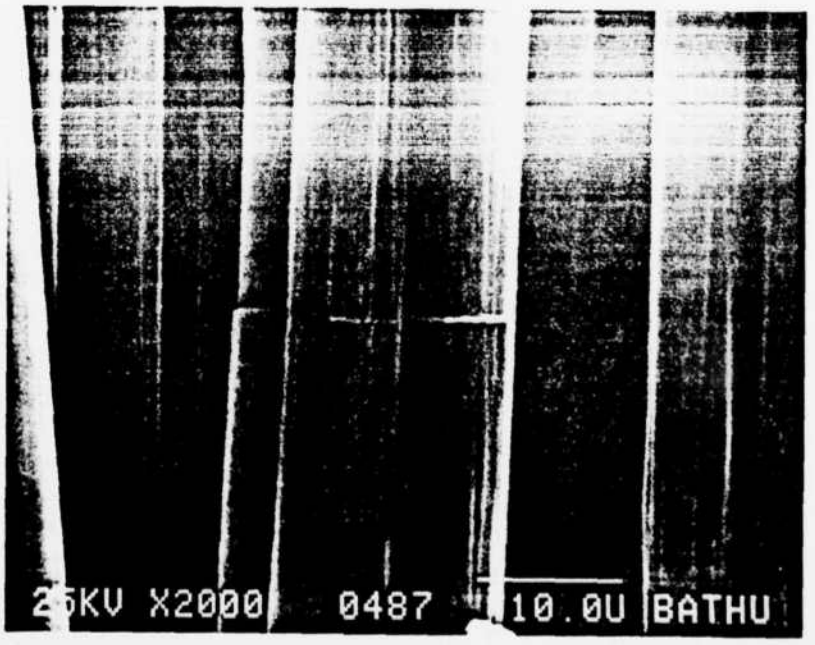

Fig. 22. Details of multiple fiber fractures in $[0,0]_s$ laminates.

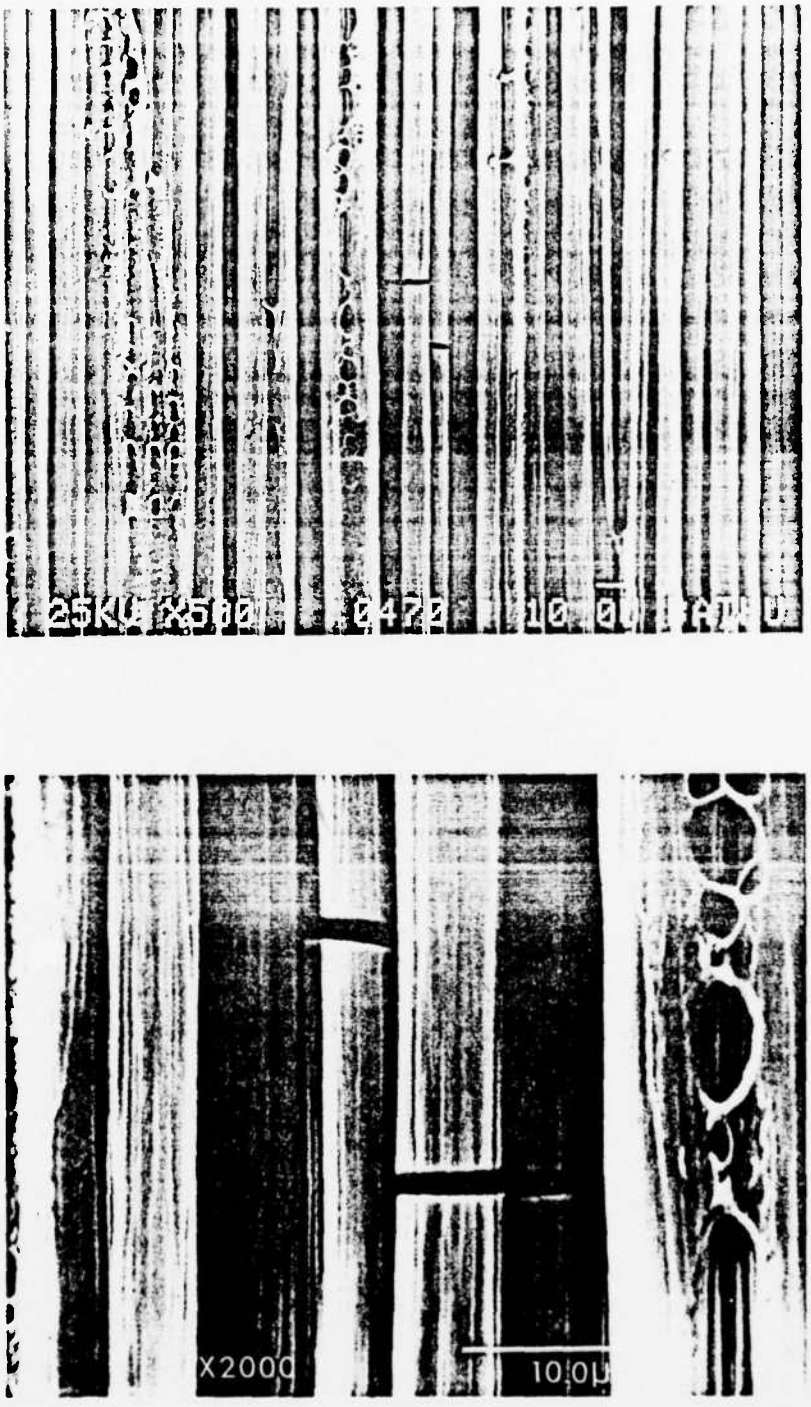

Fig. 23. Details of multiple fiber fractures in $[0,0]_s$ laminates.

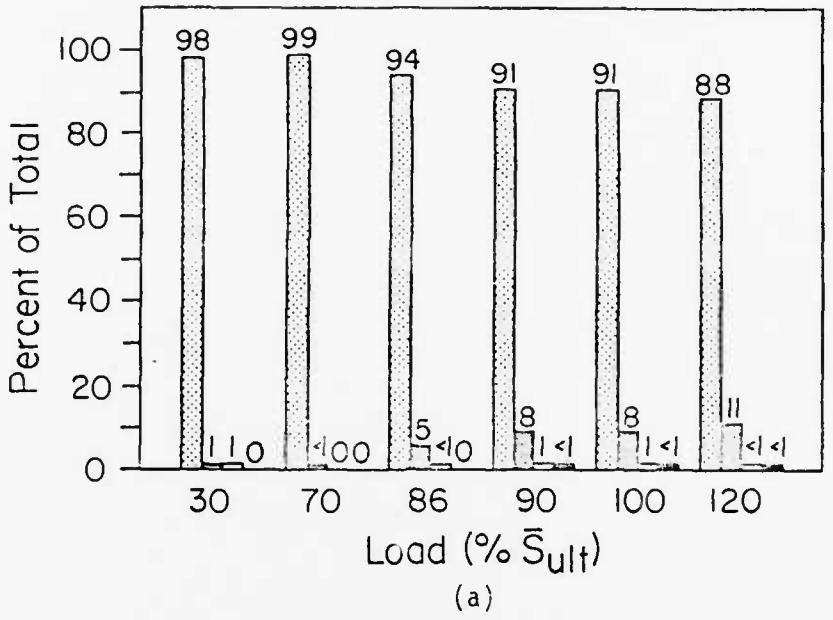

(a)

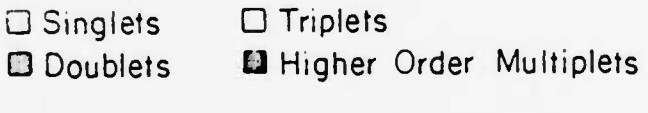

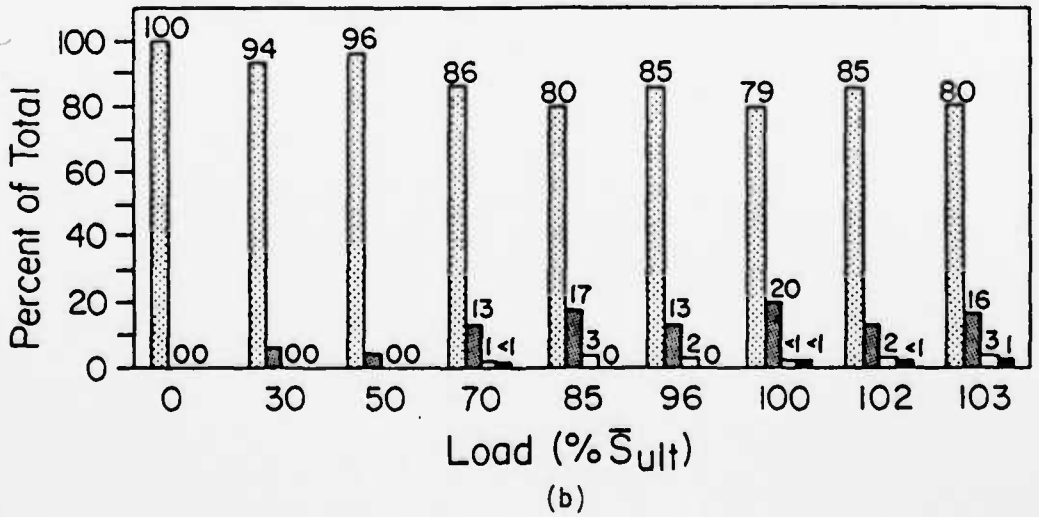

(b)

Fig. 24. Distribution of multiple fiber breaks (multiplets) for the $[0,90_2]_s$ laminates (a) and $[0,0]_s$ laminates (b).

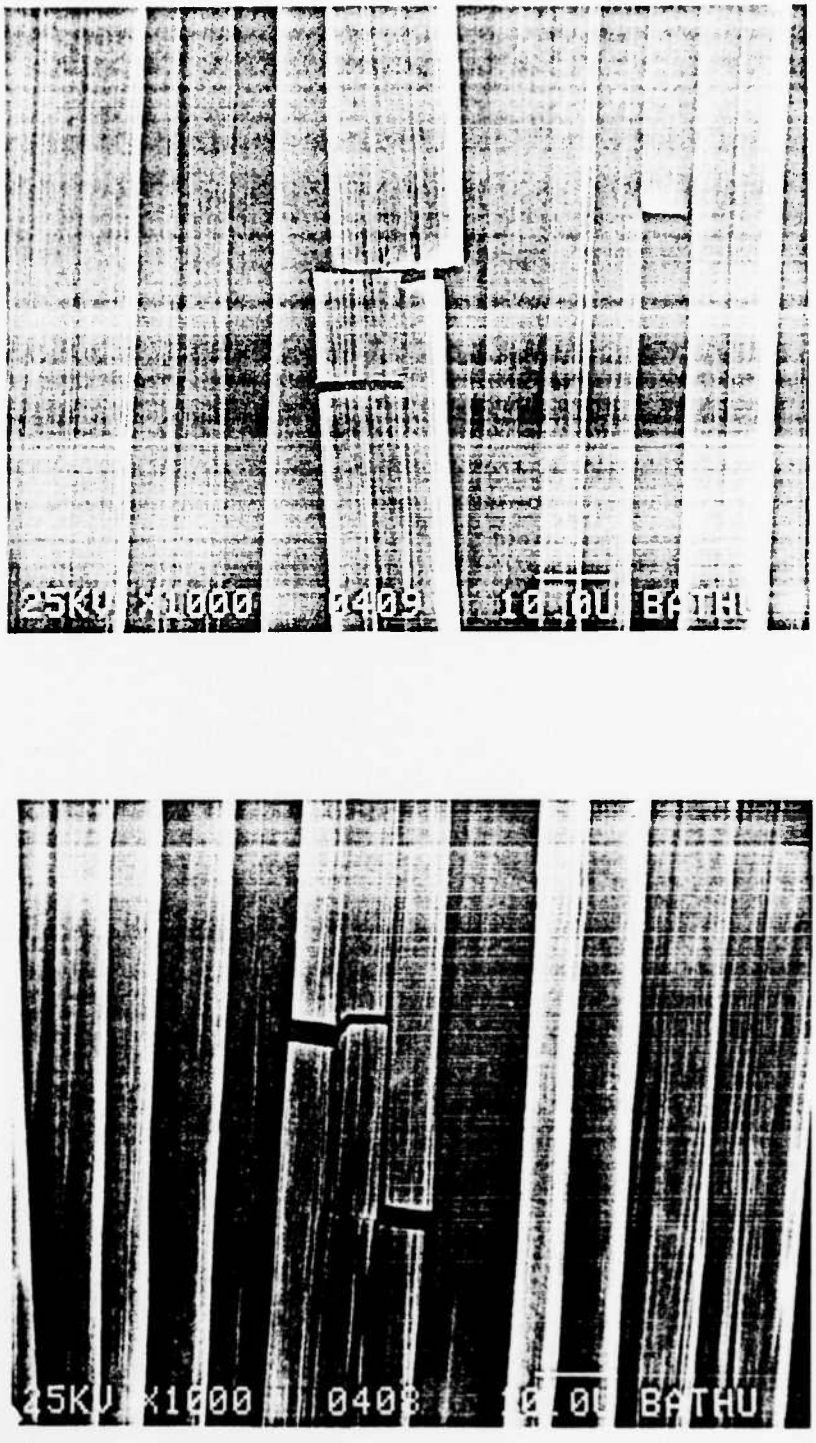

Fig. 25. Details of multiple fiber fractures in $[0,0]_s$ laminates.

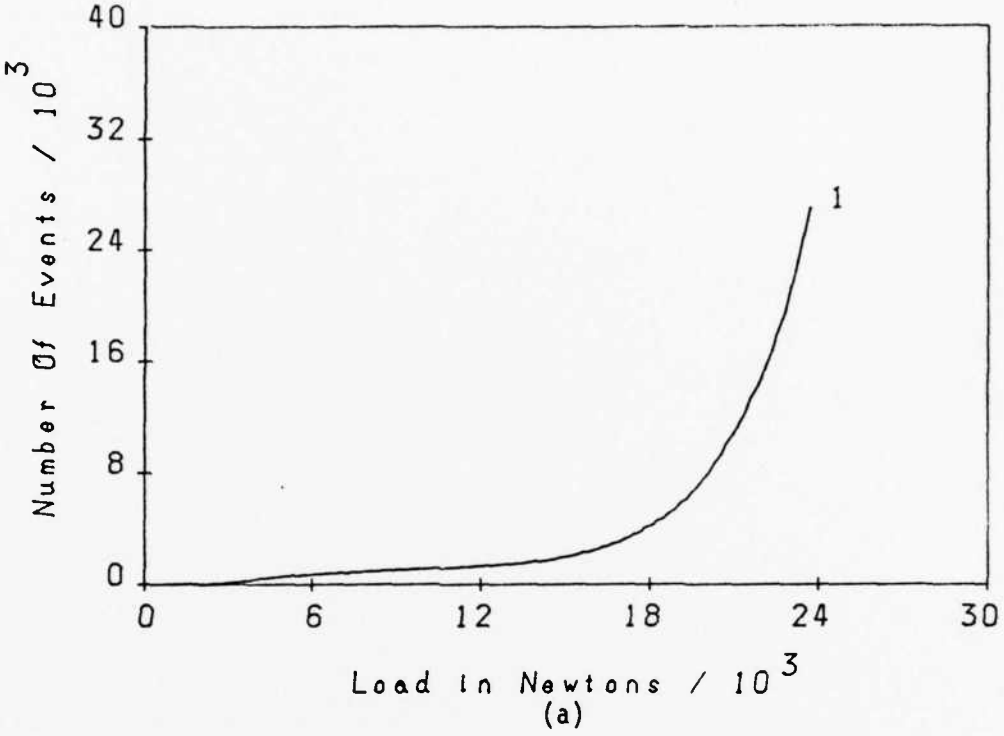

(a)

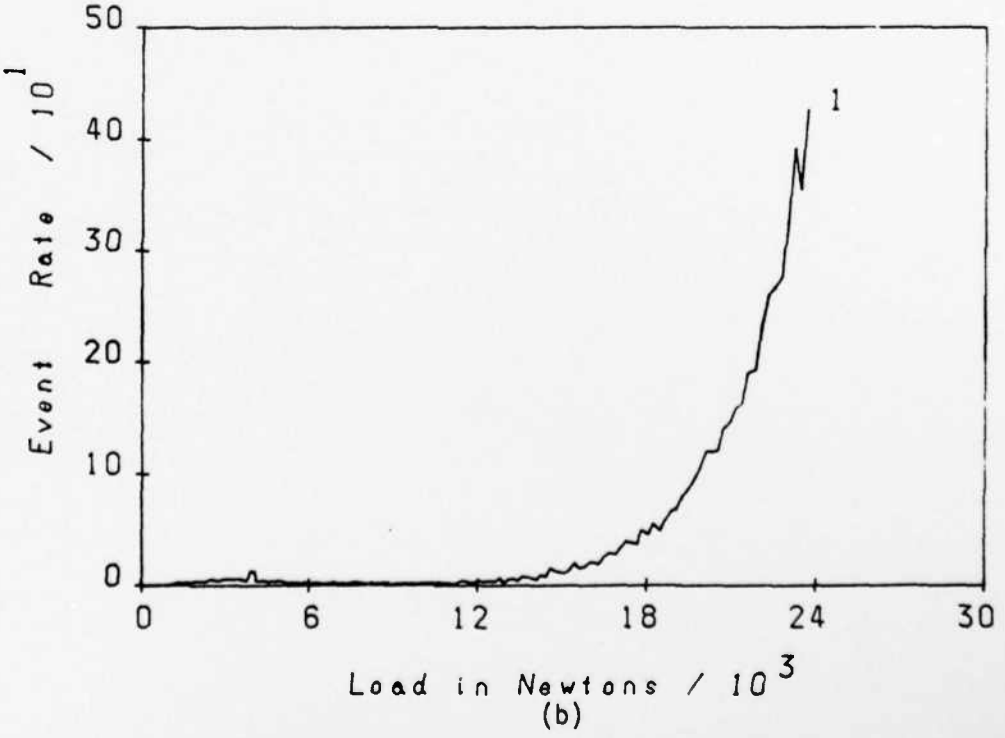

(b)

Fig. 26. Total number of acoustic emission events (a) and rate of events (b) for quasi-static loading of a typical $[0,0]_s$ specimen.

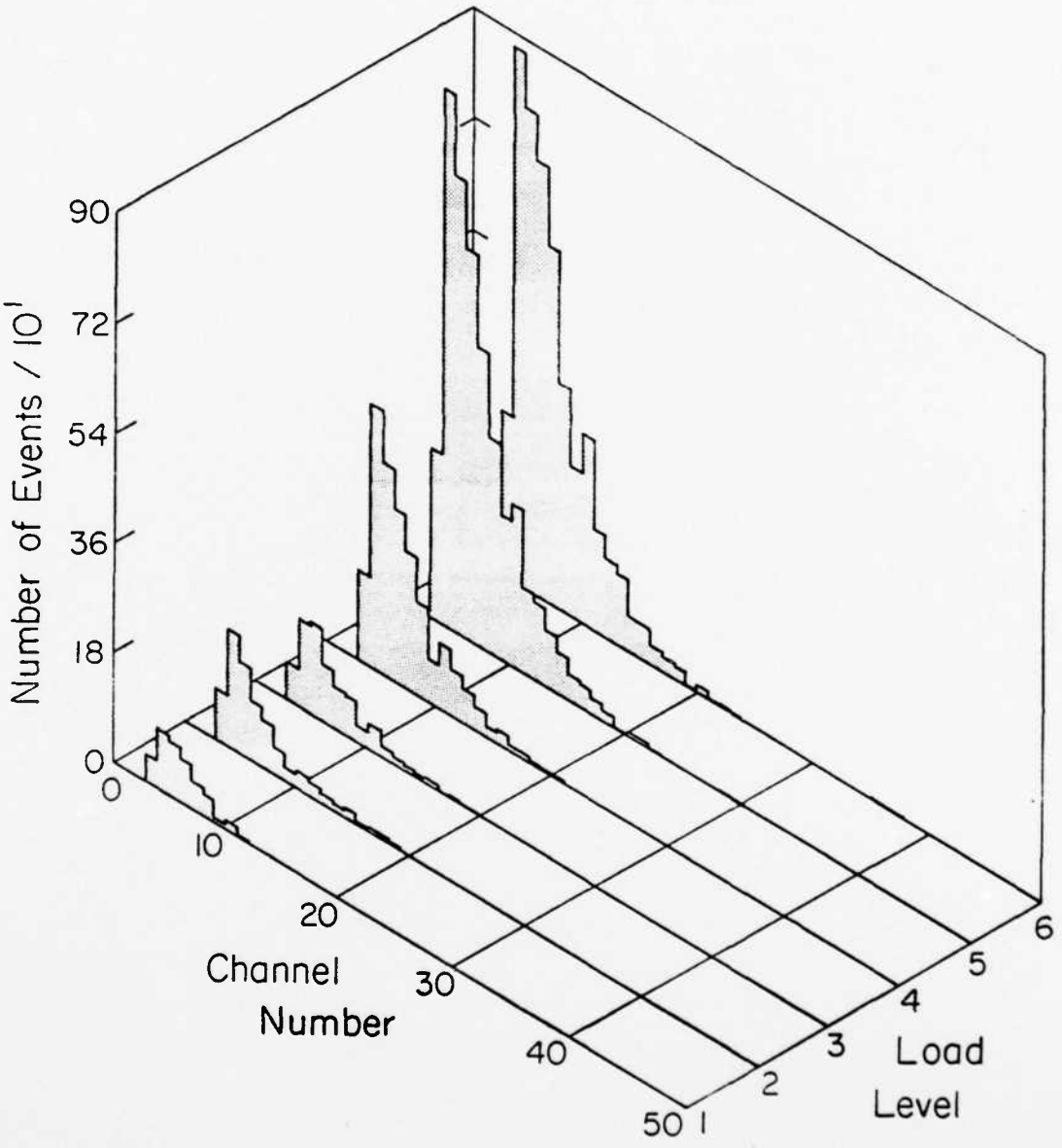

Fig. 27. Amplitude distributions by load level for a $[0,0]_s$ laminate.

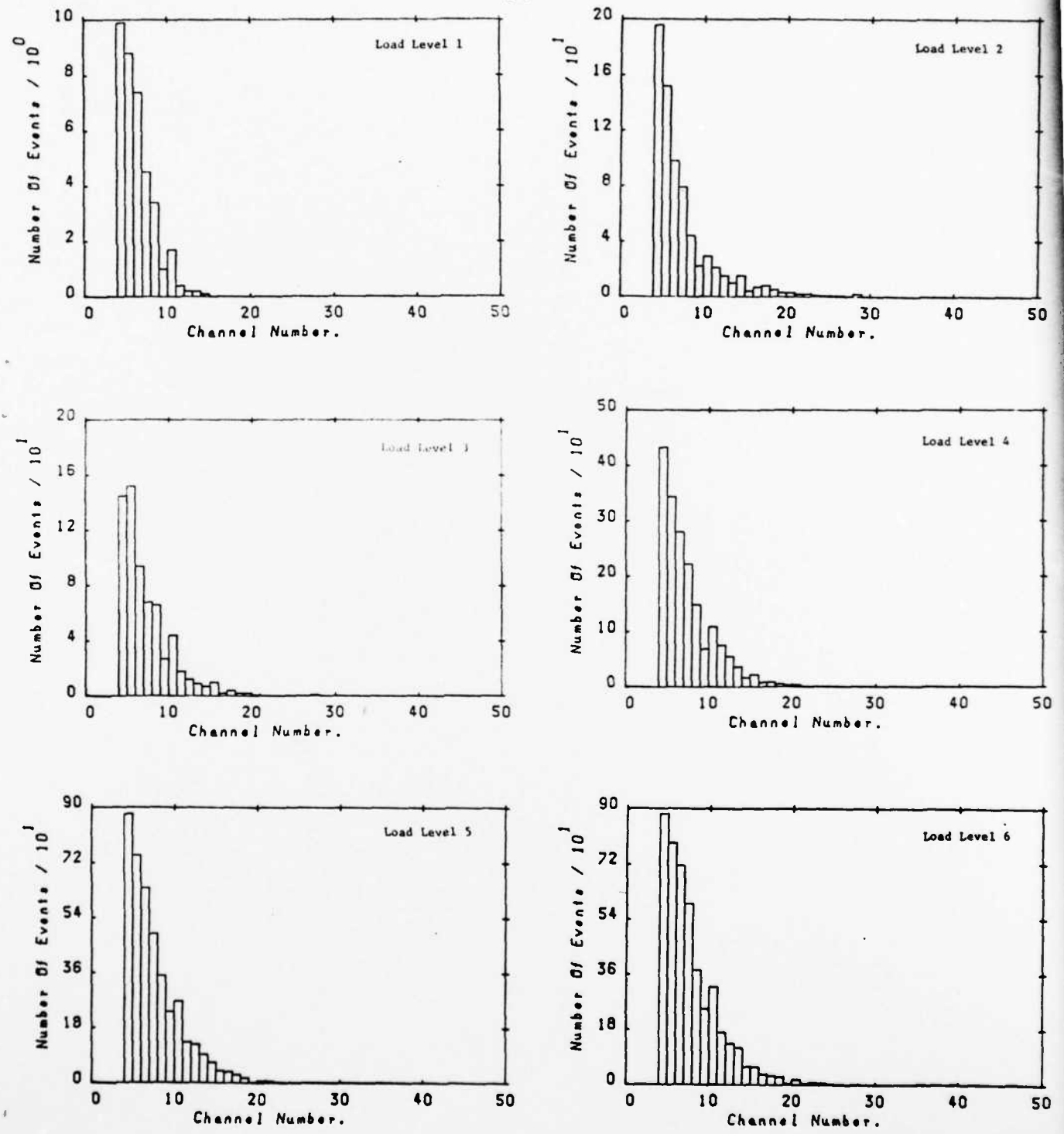

Fig. 27. (continued) Amplitude distributions by load level for a $[0,0]_s$ laminate.

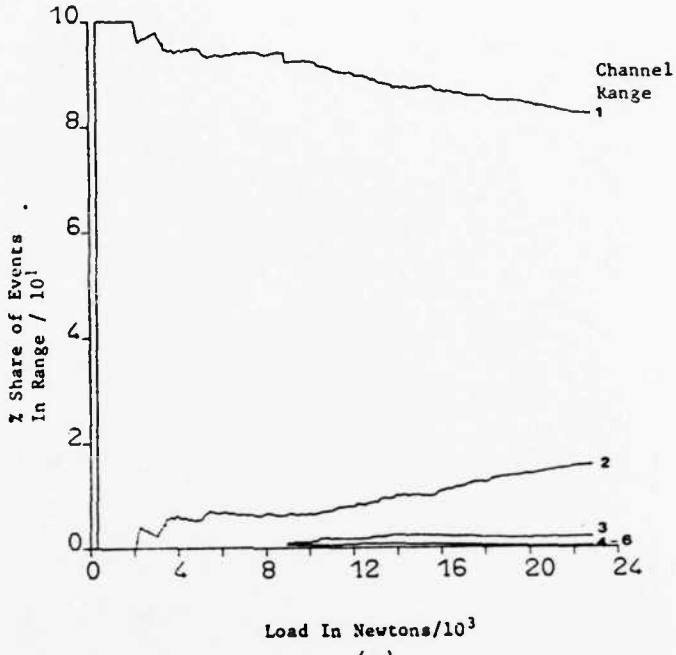

(a)

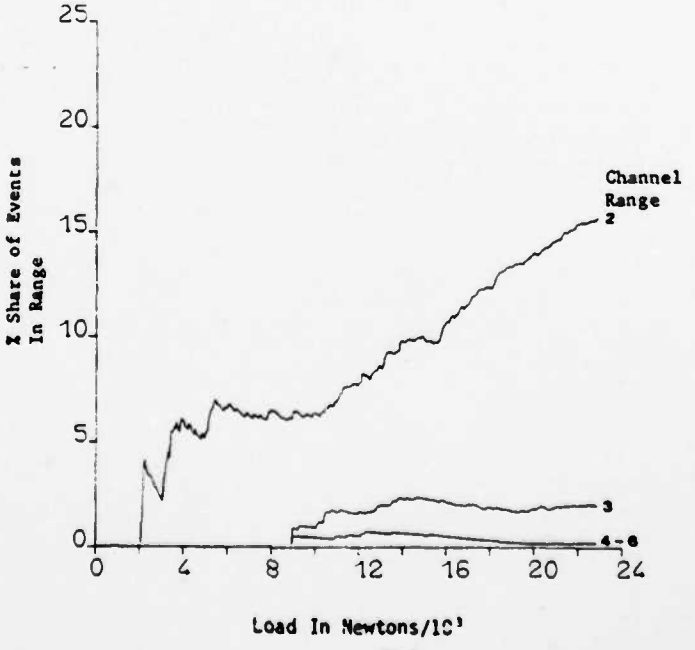

(b)

Fig. 28. Percent share of events in range for a $[0,0]_s$ laminate.
(a) Including channel range 1; (b) excluding channel range 1.

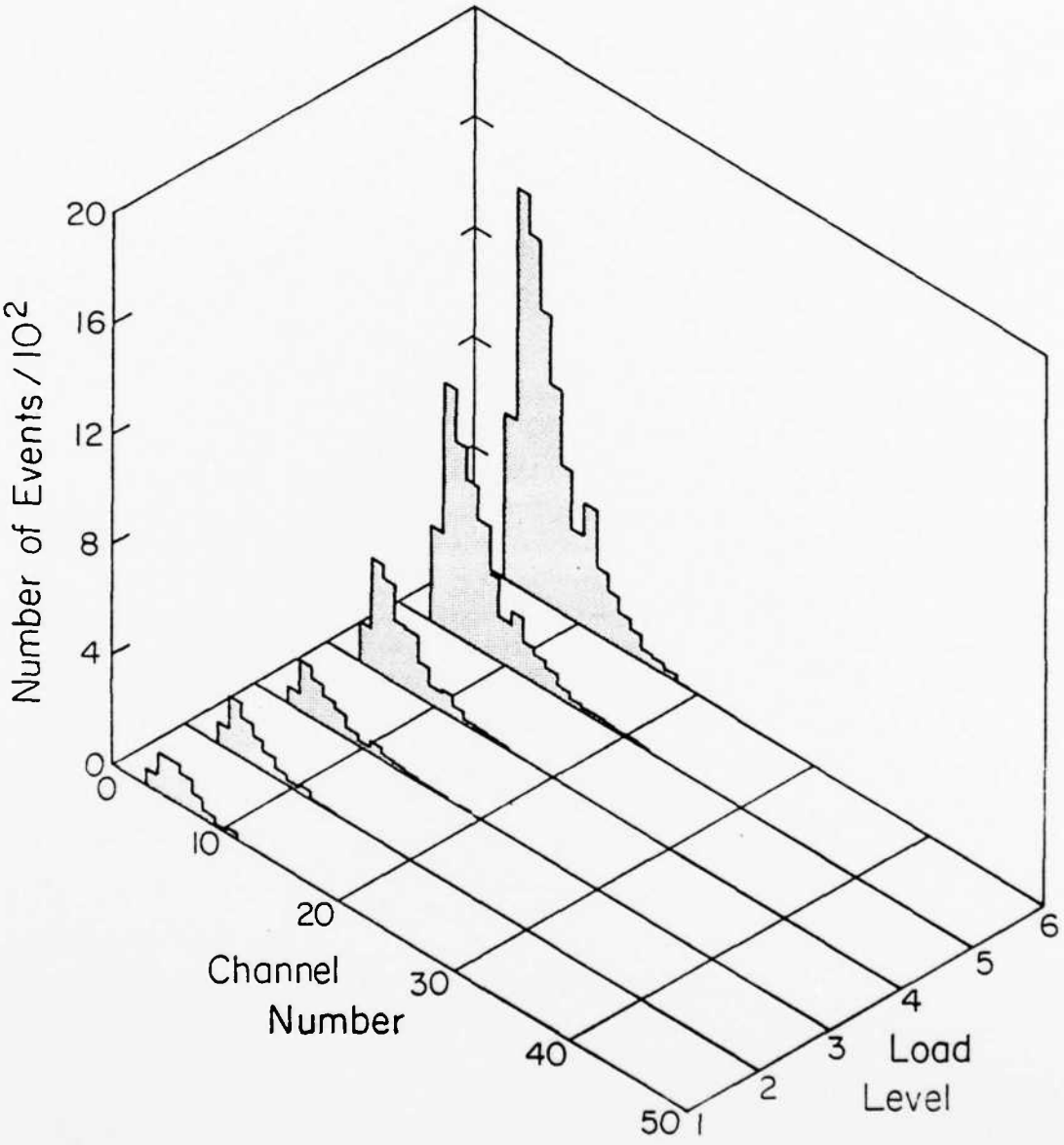

Fig. 29. Amplitude distributions by load level for a $[0,0]_s$ laminate.

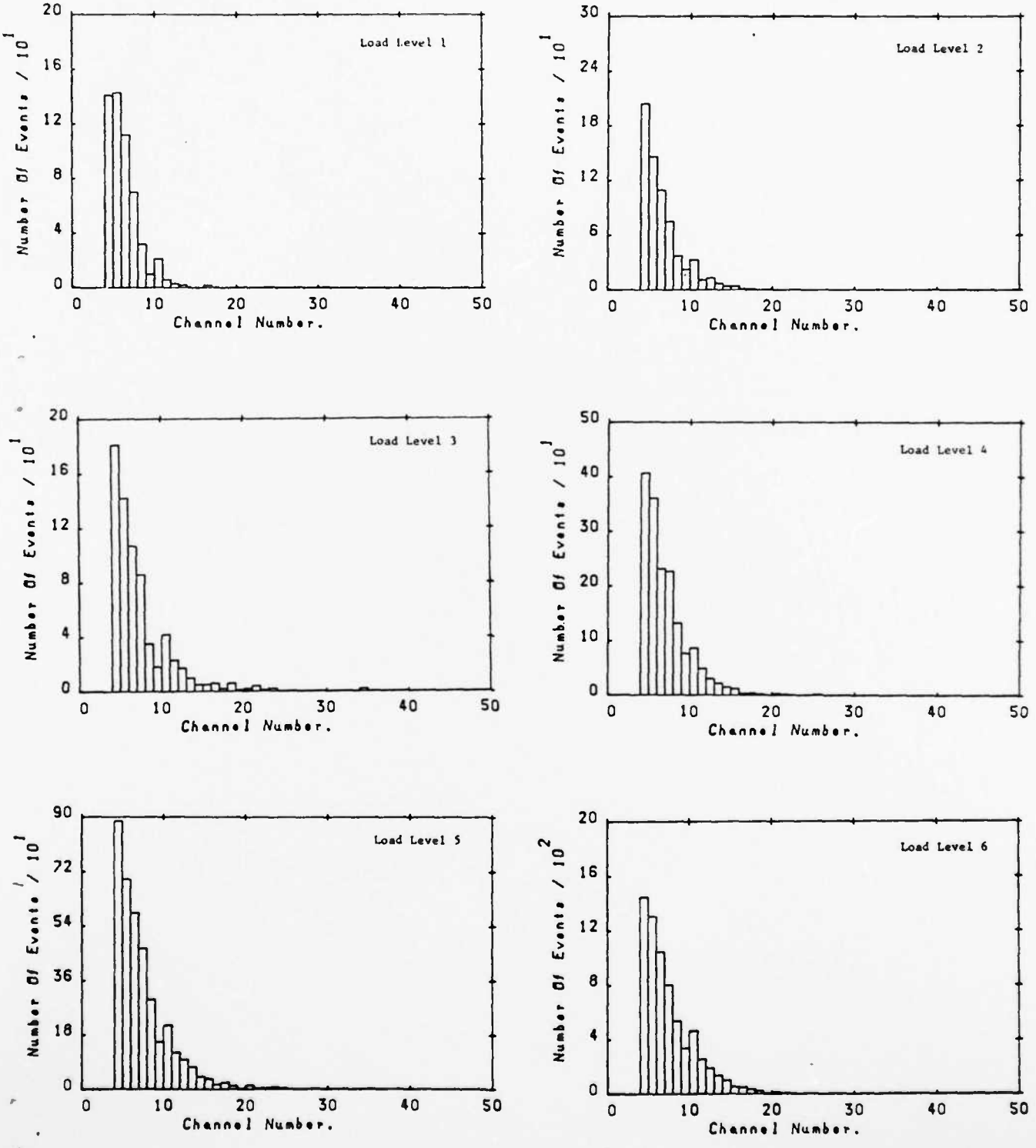

Fig. 29. (continued) Amplitude distributions by load level for a $[0,0]_s$ laminate.

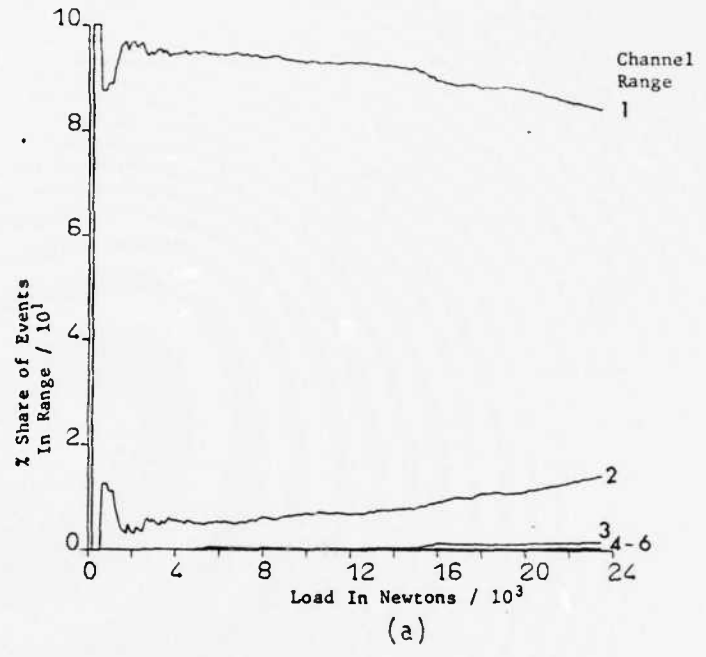

(a)

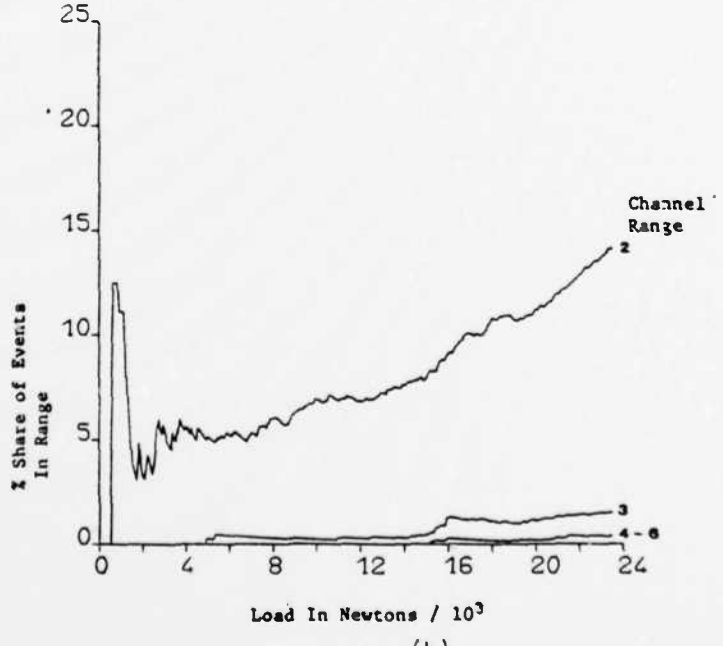

(b)

Fig. 30. Percent share of events in range for a $[0,0]_s$ laminate.
(a) Including channel range 1; (b) excluding channel range 1.

AD-A139 128 ASSESSMENT OF MICRODAMAGE DEVELOPMENT DURING TENSILE LOADING OF GRAPHITE/..(U) VIRGINIA POLYTECHNIC INST AND STATE UNIV BLACKSBURG R D JAMISON ET AL. JAN 84

2/2

UNCLASSIFIED ARO-19913.1-MS-A DAAG29-82-K-0190 F/G 11/4 NL

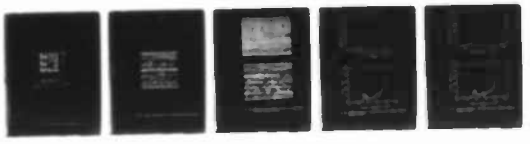

END
DATE FILMED
4-84
DTIC

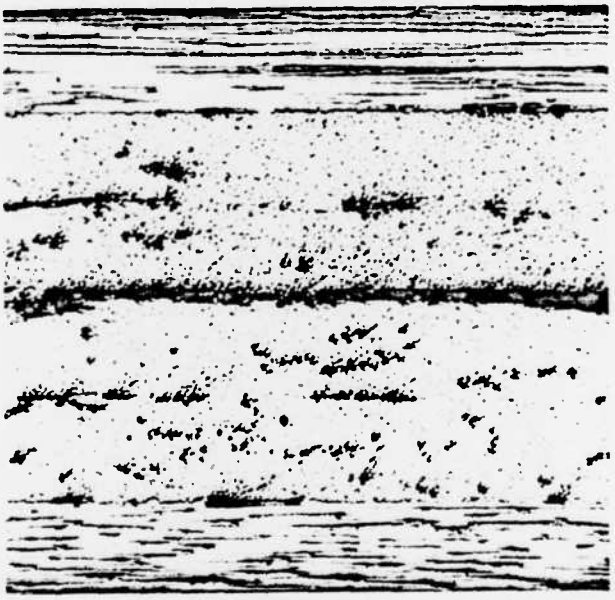

Fig. 31. Detail of edge section of a virgin porous $[0,90_2]_s$ laminate.

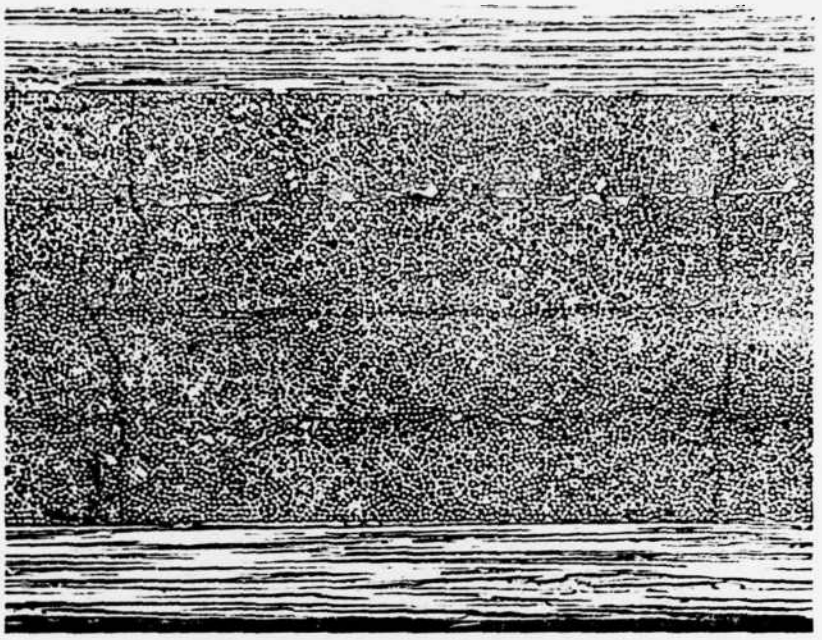

a

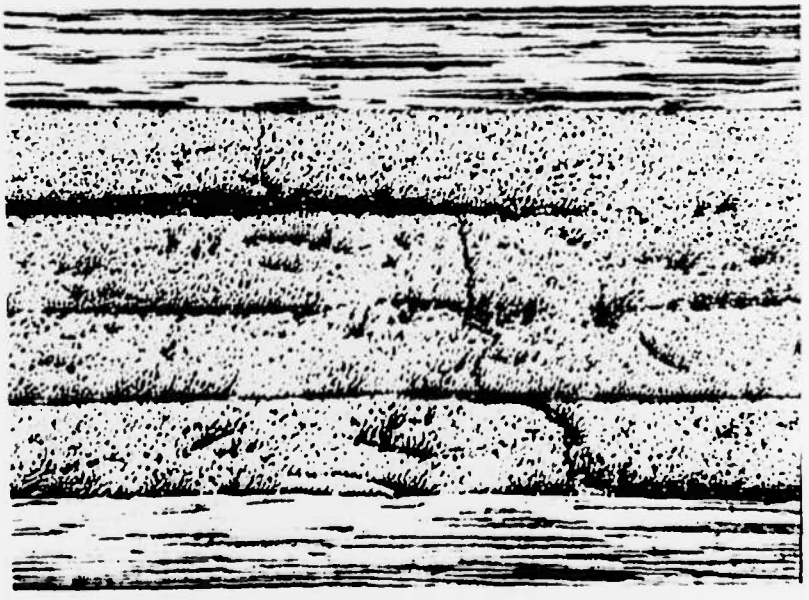

b

Fig. 32. Comparison of transverse ply cracks in (a) non-porous and (b) porous $[0,90_2]_s$ laminates.

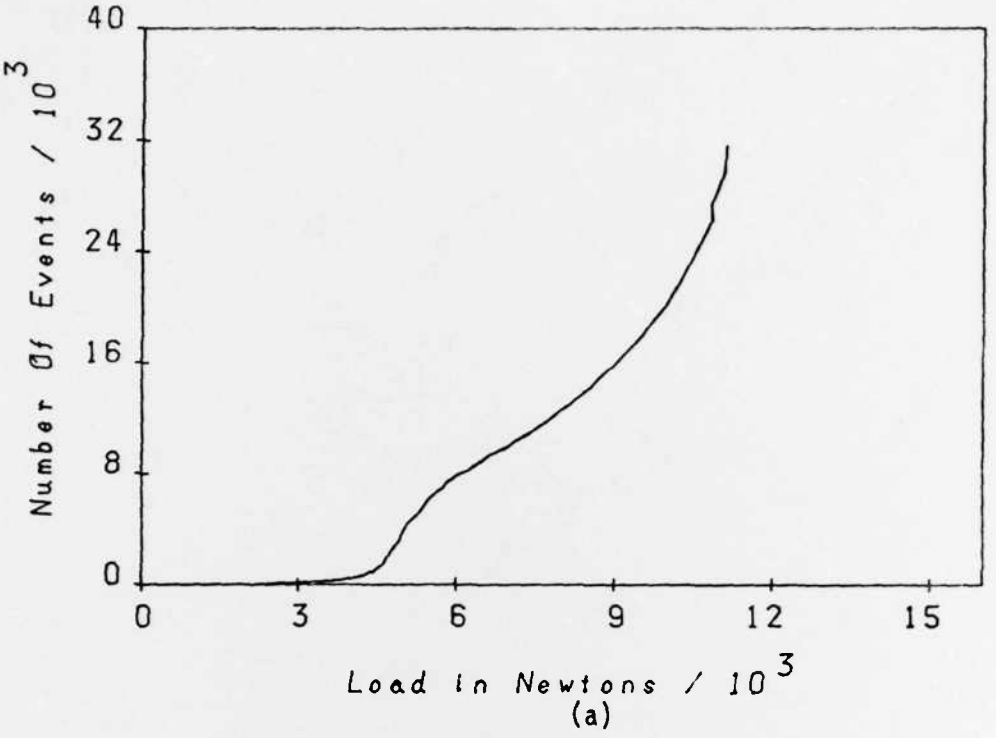

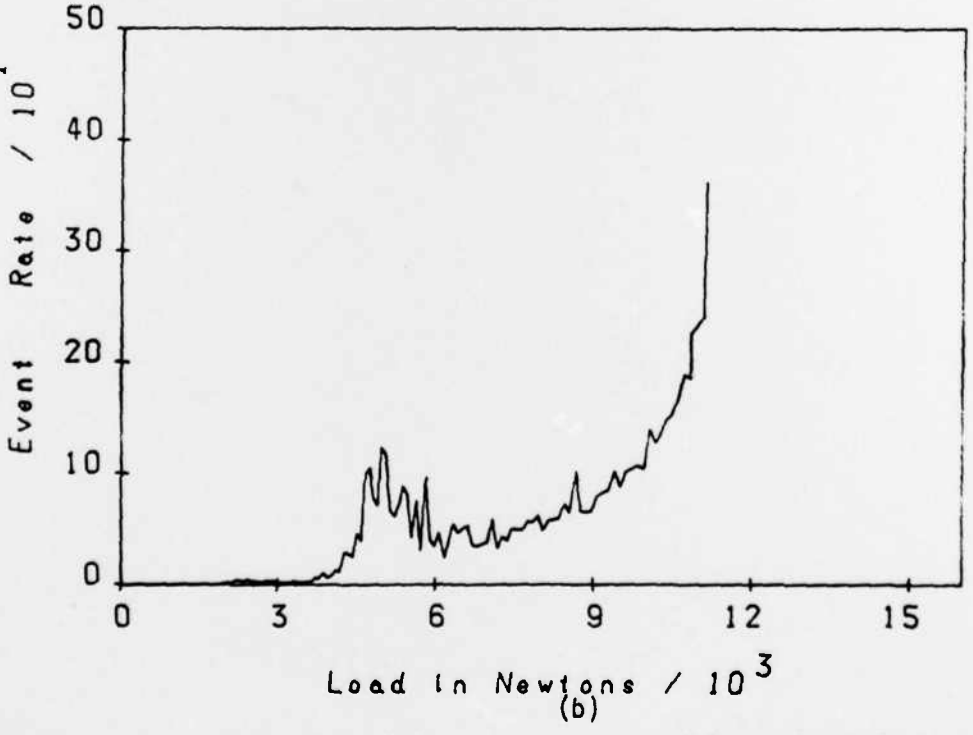

Fig. 33. Cumulative events (a) and event rate (b) vs. load for a porous $[0,90_2]_s$ laminate.

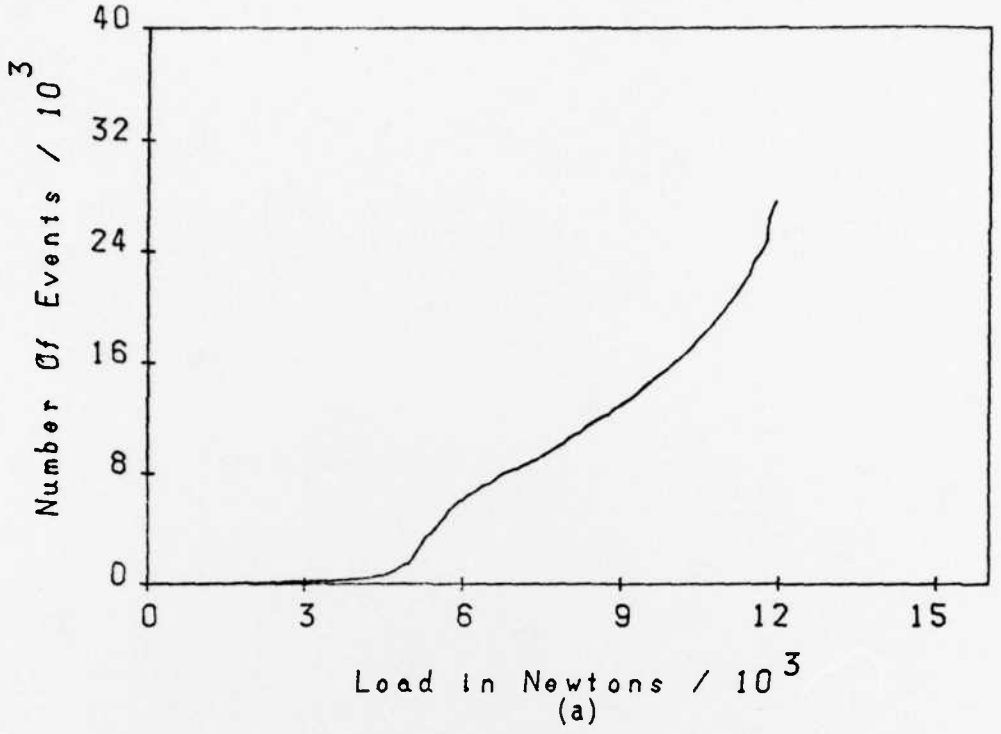

(a)

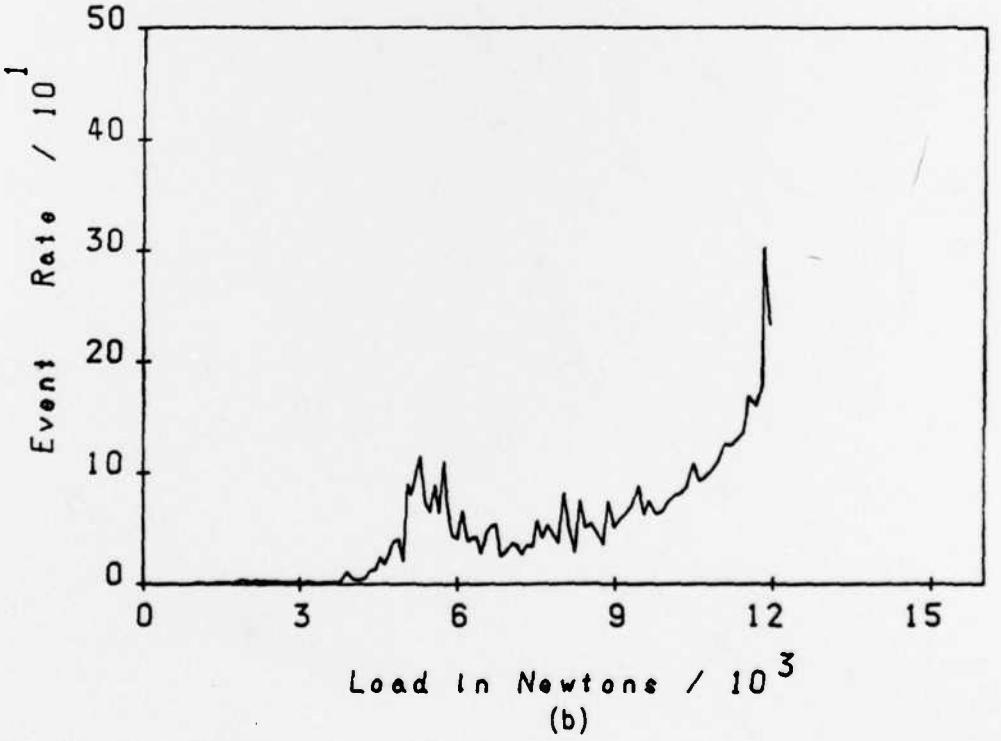

(b)

Fig. 34. Cumulative events (a) and event rate (b) vs. load for a porous $[0,90_2]_s$ laminate.


LMED